Quantification of toroid microtissue contraction using a toroid climbing assay

By

Andrew Howes

B.A., Case Western Reserve University, 2016

A thesis submitted in partial fulfillment of the requirements for the Degree of Master of Science in the Department of Molecular Pharmacology, Physiology and Biotechnology at Brown University

Providence, Rhode Island

May 2018

Declaration of Authorship

As the sole author of this thesis, I authorize Brown University to lend it to other institutions or individuals for the purpose of scholarly research.

Signed:

_____

Andrew Howes, Author

Date:

_____

I further authorize Brown University to reproduce this thesis by photo-copying or other means, in total or in part, at the request of other institutions or individuals for the purpose of scholarly research

Signed:

_____

Andrew Howes, Author

Date:

_____

Signature Page

This thesis by Andrew Howes is accepted in its present form by the Department of Molecular Pharmacology, Physiology, and Biotechnology as satisfying the thesis requirements for the degree of Master of Science

Signed: _____ Date: _____

Dr.Jeffrey Morgan, Advisor

Signed: _____ Date: _____

Dr.Edith Mathiowitz, Reader

Signed: _____ Date: _____

Dr.Toni-Marie Achilli, Reader

Approved By Graduate Council

Signed: _____ Date: _____

Andrew G. Campbell, Dean of the Graduate school

Acknowledgements

I would like to start by acknowledging my parents and the many years they have devoted to support me. Growing up whether it be driving me to practices, staying up late studying for tests, or just being there for me in times of need, I am grateful for your continuous support and motivation.

Next I would like to give thanks to all the people at Brown who have mentored me and helped to make this thesis possible. Starting with Dr. Jeffrey Morgan, thank you for giving me the opportunity to join the Morgan Lab and helping me to mature as a scientist and intellectual. Elizabeth Leary, for showing me the ropes and training me in how to first make my first microtissues. Benjamin Wilks and Kali Manning, for taking me in and guiding me through graduate school and the lab. Thank you for always being a great source of insight and helping me to grow in the lab. You have all played an integral role in this thesis and making it achievable.

Contents

List of Figures

List of Tables

List of Symbols

$Position_{Ramp}$	distance	µm
D_{in}	distance	µm
A_{Lumen}	area	μm^3
$Triangle_{Base}$	distance	µm
$Thickness$	distance	µm
$D_{Microtissue}$	distance	µm

Abstract

The advancement of three dimensional biological techniques, such as microtissues, allows for the more accurate representation of *in vivo* structures. Yet, the added dimension pushes the limits of traditional analysis techniques. As such, there is a need for new quantitative assays for three dimensional tissues. Using non-adhesive agarose molds, microtissues such as spheroids and toroids can be created. Upon seeding into toroid shaped molds, cells self-assemble and naturally contract in a circumferential manner around a peg. These toroid microtissues can then be used as building blocks for biofabrication and or *in vitro* models.

The toroid climbing optimization assay was developed to utilize this circumferential contraction and direct it within specifically designed non-adhesive agarose molds to quantify microtissue assembly. For a single toroid, cells were seeded into a circular trough at the base of an angled ramp surrounding a central peg. The ramp angles varied between 45° and 75° with a length of $1\,\mathrm{mm}$. Using wide-field microscopy, cells can be seen self-assembling into toroid microtissues and contracting up the precisely designed ramps from a bottom-view. As the inner lumen diameter changes with contraction, the position of the microtissue on the ramp can be tracked over time based on the mold geometry. This provides a more high-throughput method than the current approach of side-view based on the amount of toroids that can be tracked during a single experiment. Having a more high-throughput quantitative method provides a workable approach to conduct screening assays and proof-of-concept for the scale-up to a 96-well format.

Chapter 1

Background

1.1 Cellular Forces

Cellular forces are reliant on both cytoskeleton remodeling and cell adhesion molecules produced. As the cytoskeleton remodels and generates tension, adhesion molecules tether cells to their outer surroundings such as other cells within proximity. These cell-cell interactions created by cell adhesion molecules act as environmental cues or forms of communications for individual cells, signaling down a cascade within a community of cells. Cell adhesion molecules come in two forms: cell-ECM (mainly integrins) and cell-cell molecules (mainly cadherins). Transmembrane molecules link to the ECM, creating a support that acts as a two-way communication tool, passing information such as substrate stiffness and terrain. Measuring these forces using cell-ECM interactions, a cell can change its morphology, spreading and function. Cell-cell adhesion molecules such as cadherins create adheren junctions that act as bidirectional communication mechanisms. If one cell experiences tension, a calcium influx will result in a cascade ultimately reorganizing the cytoskeleton to account for such changes in the environment. The output of force in the form of contraction from the cells will also occur as a result of reorganization. These cellular forces are believed to play integral roles in disease states, activation of fibroblasts, and other physiological states depending on cell type. Mechanical forces generated from these reactions also play essential parts in the self-assembly and self-sorting of tissue formation (Youssef (2012)).

1.2 Extracellular Matrix

The extracellular matrix (ECM) is a dynamic non-cellular micro-environment within all tissues that provides chemical and mechanical signaling required for morphogenesis, differentiation and homeostasis. Each tissue consists of a distinct ECM topology for required function, however, a generic ECM is composed of water, proteins, and polysaccharides. With the ECM being highly dynamic, it undergoes constant remodeling enzymatically or non-enzymatically. The ECM is coupled to adhesion molecules of the cytoskeleton creating cell-ECM interactions that direct morphological and physiological function. Physiological function can be controlled by growth factors binding with cell-surface receptors resulting in a signal (Frantz, Stewart, and Weaver (2010)).

1.3 3D Biology

The study of three-dimensional (3D) biology is of growing interest as researchers are learning that it provides more relevant information when compared to two-dimensional (2D) cell culture. 3D cell culture provides an innate environment more closely related to a living organism by promoting cell-cell interactions not seen in 2D cell culture(Abbott (2003)). Many techniques for 3D cell culture utilize either a natural or synthetic scaffold to allow cells to form 3D structures for experimentation. This method has produced positive results for the replacement of injured tissue or drug delivery methods, however, dense scaffold architecture creates extensive cell-scaffold interactions. The contrary is seen in organic tissue where cell-cell interactions outweigh cell-scaffold interactions.These cell-cell interactions allow for the synthesis and assembly of an extracellular matrix (ECM) with a high cell density. Therefore, scaffolds within microtissues account for a large amount of the overall mass, reducing cell density and reliance of microtissue assembly on cell-cell interactions. Due to these pitfalls, researchers begun turning their efforts to scaffold-free approaches (Abbott (2003), Elizabeth Leary (2017)).

Scaffold-free methods allow cells to go through a process called self-assembly. It is thought that self-assembly mimics natural processes found in embryogenesis, morphogenesis, and organogenesis (Dean et al. (2007)). When microtissues are self-assembling from monodispersed cells, cell-cell interactions are the key driving force. The heightened cell-cell interactions and cell density in self-assembled tissues provides a relative in vivo approach when compared to native tissues.

During self-assembly, monodispersed cells will spontaneously form spheroid structures. There are many non-scaffold methods to form spheroid microtissues from monodispersed cells such as, hanging drop, spinner culture, pelleted suspensions, and agitation in micromilled recesses. In order to further study the intricate possibilities of self-assembled microtissues, the Morgan lab at Brown University developed a method to form micromolded non-adhesive agarose gels (Fig. 1.1) (Dean et al. (2007)).

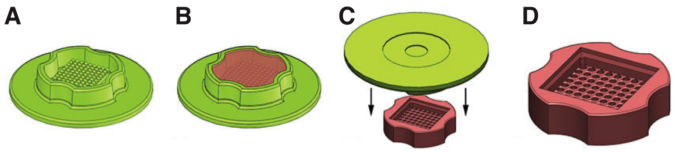

Figure 1.1: Casting of non-adhesive agarose molds using 3D Petri Dish. (Elizabeth Leary, 2017)

1.3.1 Self-assembly of Complex Microtissues

By using micromolded non-adhesive agarose gels in the shapes of rods, toroids, and honeycombs, the self-assembly of structures more complex than a spheroid were studied. Two cell types, normal human fibroblasts (NHFs) and rat hepatomas (H35s), were used to study morphological and stability changes while forming complex structures. Here, it was observed that monodispersed NHF and H35 cells seeded in complex molds were able to form stable complex microtissues. H35s were able to form rods, tori, and honeycombs. NHFs were able to form rods and toroids, however, cells were unsuccessful in forming honeycomb structures. A key observation was the rate of contraction by the NHF and H35 cells in 3D cell culture. It was

noticed that the NHFs contracted to spheroid structures at a higher rate than that of the H35 cells. The higher contraction levels and surface tension in the NHFs suggest why the NHFs were unable to form honeycombs and the less contractile H35 cells could (Fig. 1.2).

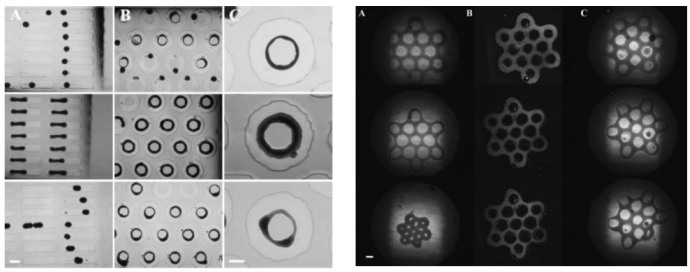

Figure 1.2: Formation of complex microtissues such as rods, toroids, and honeycombs in non-adhesive agarose molds. (Dean et al., 2007)

In order to further investigate contractility, a 1:1 mix of NHFs and H35s were seeded in the complex molds with a fluorescent dye. It was observed that the mixture underwent self-sorting during self-assembly, where the more contractile NHFs were enveloped by the less contractile H35s. It was also seen that NHFs had different morphologies in the mixture when under mechanical stress (Fig. 1.3).

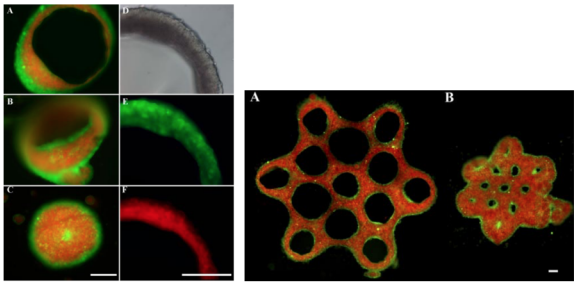

Figure 1.3: Self-Sorting of hybrid NHF and H35 complex microtissues. (Dean et al., 2007)

Overall, it was proven that monodispersed cells seeded in complex molds can create complex tissues and the contractility of the individual cell type plays an important role in their successful formation (Dean et al. (2007)).

1.3.2 Dynamics of Self-Assembled Microtissues

After seeing that cells undergo self-segregation during self-assembly within complex micromolded non-adhesive agarose gels, further studies were conducted to test the dynamics of heterotypic microtissue environments (Dean et al. (2007)). It was learned that seeding density and well dimensions of the micromolds play an integral role in controlling and determining the viability of the microtissue (Fig.1.4). To test how seeding density and well diameter factored in tissue formation, NHFs were seeded within non-adhesive agarose molds of $200\,\mu\mathrm{m}$, $400\,\mu\mathrm{m}$, and $600\,\mu\mathrm{m}$ diameter. These wells either had flat or hemisphere-shaped bottoms. It was observed that molds with hemispherical shaped bottoms, funneled cells together in a more concise manner compared to flat bottom wells. The flat bottom molds often created individual spheroid clusters within the wells.

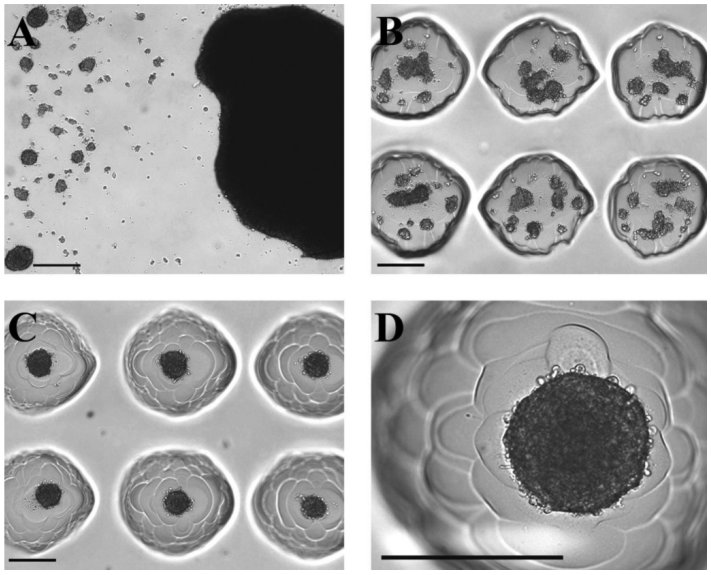

Figure 1.4: Effects of recess geometry on microtissue self-assembly. (Napolitano et al., 2007)

To study self-aggregation, a single cell suspension of fluorescent stained HUVECs was seeded and allowed to form spheroid structures. After a week, the spheroids were seeded with a fluorescent labeled NHF suspension. Using the fluorescent labeling to track cell location, the spheroids underwent reorganization where the more contractile cell suspension, NHFs, segregated to the core of the spheroid.

This finding showed that microtissues are able to reorganize after being allowed to mature and are fluid structures (Napolitano et al. (2007)).

To study the behavior of more complex microtissues, toroid microtissues were then formed at varying seeding densities and circumferences by creating new mold designs. The toroids contracted around a central peg to form a viable structure. Over the course of five days, it was noticed that the toroid thicknesses had decreased, creating a thin sleeve around the mold peg. A minority of toroids had begun to move up the pegs and out of their wells completely as well as break under tension inside the wells. This observation further indicated that cellular contraction and tension are important for the self-assembly of complex shapes such as toroids (Blakely et al. (2015)).

1.3.3 Tissue Fusion and Cell Sorting

Knowing that self-sorting during self-assembly is not terminal (Blakely et al. (2015)), new studies were conducted to understand whether self-sorting can be controlled and the fusion of microtissues could occur. Monodispersed NHF cell suspensions were allowed to mature to spheroids for either 1, 4, and 7 days and then added to a rod shaped mold. In doing so, the fusion kinetics of these spheroids could be studied. Rate of fusion, coherence of the spheroid building blocks, and length of the rod formation could be controlled by mold structure. It was observed that the more mature spheroids fused at a slower rate, had less coherence, and increased length of rod microtissues.

It had previously been shown that cells were able to self-sort even after maturation (Napolitano et al. (2007)). To test the control of cell sorting by maturation, two cell suspensions, NHF and H35, were tested using the previous experiment of spheroid maturation. spheroids were cultured for 1, 4, and 7 days. The cell positioning was tracked using fluorescent labeling and revealed that 1 day pre-cultured spheroids readily underwent reorganization when mixed. However, this pattern was not the same for the four and seven day pre-cultured spheroids. It was discovered that NHF spheroids fused with H35 spheroids, but certain areas of the

microtissues resulted in H35s being dispersed within the core of the fused structures and NHFs lining the outside.These new observations suggested that by using pre-formed microtissue building blocks, cell structures might be able to maintain their viability when forming larger heterotypic microtissues (Fig.1.5) (Rago, Dean, and Morgan (2009)).

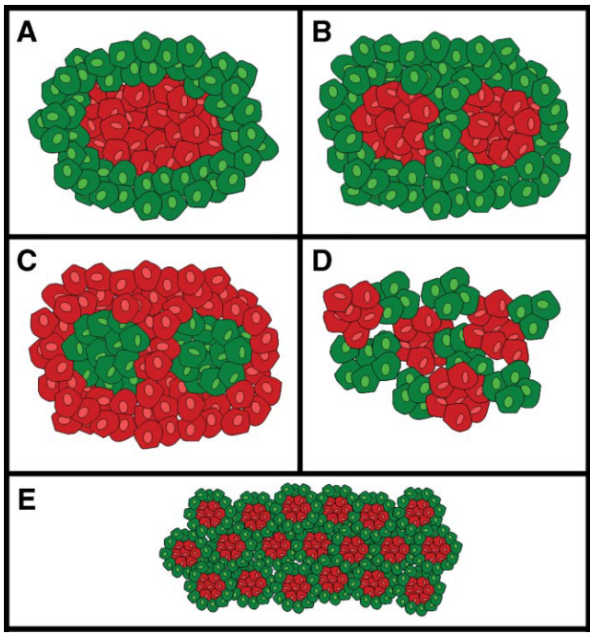

Figure 1.5: Cell sorting of pre-cultured H35 and NHF spheroids. (Rago, Dean, and Morgan, 2009)

1.3.4 Cell-Derived Tension in Self-Assembly

The observation that contraction and tension play an important role in the process of self-assembly lead to the examination of dog-bone microtissue structures (two toroids fused together by a rod). Previous studies have shown that contraction and tension can lead to complex microtissue failure and morphology change (Napolitano et al. (2007)). NHFs were allowed to self-assemble into dog-bone structures, where the structures eventually failed, resulting in two toroids as expected (Fig. 1.6). These models allowed for the close examination of defined and reproducible microtissue failures. In order to track cell movement and morphology, fluorescently labeled NHFs were mixed with unlabeled NHFs. It was found that as cells

elongated under tension, dendritic extensions that had formed during self-assembly began to retract, leading to mechanical failure (Dean, Rago, and Morgan (2009)).

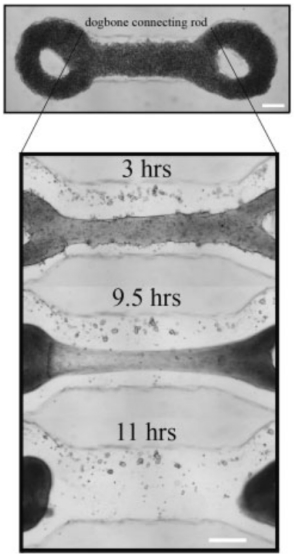

Figure 1.6: Culturing and mechanical failure of dog-bone microtissues. (Dean, Rago, and Morgan, 2009)

To test what was influencing the microtissue contraction, various pharmacological agents were added to influence contraction such as blebbistatin and Y-27632. This revealed that the dog-bone microtissue failures were strongly dependent on myosin II activation and Rho Kinase-mediated contraction. Overall, these studies provided information on cellular responses as a result of mechanical forces exerted by cells. Mechanical forces were created as a result of cell-cell interactions, again emphasizing the importance of high seeding density environments that allow heightened cell-cell interaction (Dean, Rago, and Morgan (2009)).

1.3.5 Quantifying Microtissue Kinetics

Microtissue structures were qualitatively observed undergoing contraction and other mechanical stresses in previous experiments (Blakely et al. (2015), Dean et al. (2007), Napolitano et al. (2007), Tejavibulya et al. (2011)). To further understand the kinetics of microtissues, quantitative assays to define fusion and other local phenomena that occur due to cell-cell interactions needed to be designed.

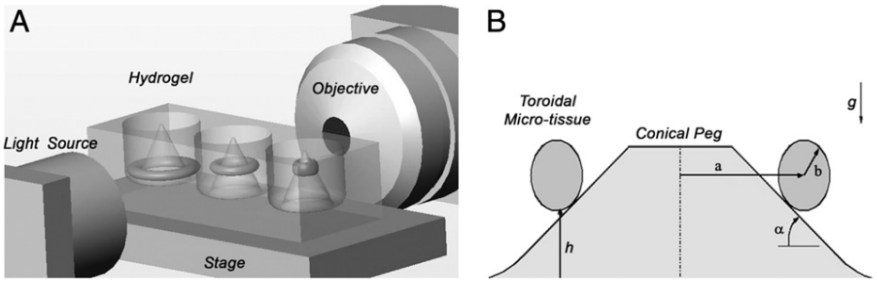

Figure 1.7: Setup for side-view imaging of toroid contraction. (Youssef et al., 2011)

In order to track the climbing of toroid microtissues, a new experimental system was created along with new angled molds (Fig. 1.7). The idea was that, once cells were seeded within polyacrylamide gels of 300, 350 and 400 um diameters, they would self-assemble into toroid microtissues. Once assembled, the toroids would naturally begin to contract up a sloped cone of either $55°$, $65°$, or $85°$ with ramp lengths of 600, 650, and 780 um respectively. The height traveled by the toroid along with major and minor axis was tracked. Over the course of 8 hours, the toroids' movements coincided regardless of mold angle. To compare the contraction of two different cell types, NHFs and H35s were seeded separately into the experimental setup. NHFs being the more contractile cell type, rapidly climbed the cone. However, H35 toroid microtissues were much slower when climbing the peg and speeds were dependent of the specific cone angles. The higher the cone angle, the slower the climbing of the H35 toroid microtissues. In order to quantify this difference of contraction speed, power output against gravitational force was used.

Using power output as a metric in conjunction with contraction, cell-cell interactions were quantified and elaborated on the role of contraction in formation. Power output was defined as the the amount of work performed against gravity to move a toroid of a known mass to a given height on an inclined polyacrylamide cone. With this definition, the power output of NHF and H35 toroid microtissues was studied by manipulating cytoskeletal-mediated contraction (Youssef et al. (2011)). Past experiments had indicated that by manipulating Rho-Kinase-mediated contraction, contraction could be inhibited (Dean, Rago, and Morgan (2009)). To continue off of these findings, toroids were treated with Y-27632, a known inhibitor

of Rho-Kinase. Based on the definition of power stated, it was found that when treated with Y-27632, toroids had a >50% decrease in power output when compared to the untreated controls. This finding emphasized the idea that cytoskeletal-mediated contraction directs the process of self-assembly (Youssef et al. (2011)).

To continue the understanding of cytoskeletal-mediated contraction in self-assembly, NHFs, H35s and 1:1 ratio toroid microtissues were treated with transforming growth factor Beta 1 (TGF-B1). TGF-B1 is know contributor to contraction of the extracellular matrix (ECM). When comparing the TGF-B1 treated tissues to the controls (NHF and H35 alone), power output increased 2-fold. Interestingly, untreated 1:1 heterotypic mixture showed a 5-fold increase in cell power. When treated with TGF-B1, the heterotypic microtissue power output increased 22-fold. This revelation expanded on the idea that not only is cell-cell interaction important in self-aggregating homotypic microtissues but also the formation of heterotypic microtissues. With this data, the understanding of heterotypic cellular forces in the formation of larger tissues can be broadened (Youssef et al. (2012)).

1.3.6 Toroid Microtissue Building Units

With the development of self-assembling high cell density microtissues, they lend themselves for use as building blocks to construct macrotissues. A main limiting factor for the creation of larger tissues is the diffusion of nutrients and wastes to and from dense tissues. After the successful construction of individual toroid microtissues, the prospect of using toroids as minimal building units was investigated (Blakely et al. (2015),Dean, Rago, and Morgan (2009)). Due to toroids containing a lumen, it was hypothesized that multiple toroid building blocks could create a porous, high cell density tissue when fused (Livoti and Morgan (2010)). By having a lumen, a higher seeding density can be used because critical diffusion is not defied.

To study the adjacent fusion of 2 toroids, pairs of NHF toroids were placed adjacent to one another on flat agarose and allowed to fuse. The rate of fusion was

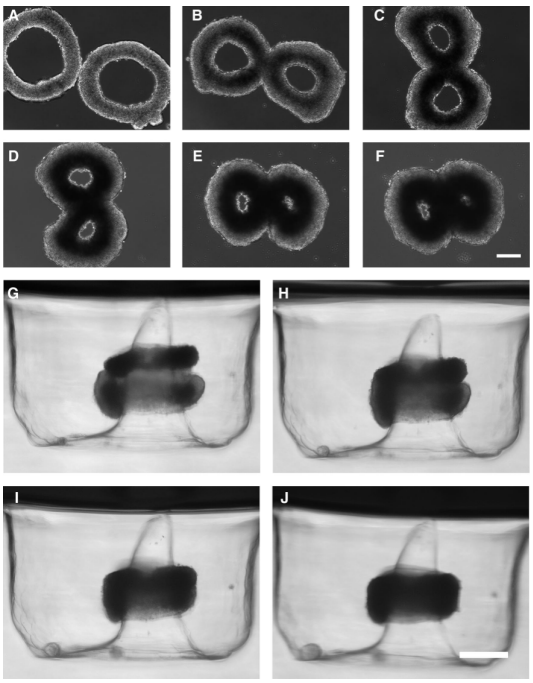

Figure 1.8: Image of adjacent toroid fusion and toroid fusion by stacking.(Livoti and Morgan, 2010)

studied by measuring the intertoroid angle, with the pair of toroids eventually forming a double lumen microtissue. Random fusion was tested by adding multiple toroids to a single agarose well. After settling at the base of the well, it was observed that many toroid lumens had aligned along the z-axis(Fig. 1.8). The toroids were allowed to culture for 7 days, where they eventually contracted to spheroid structures (Livoti and Morgan (2010)).It was shown that toroids have the capability to form larger microtissues with aligned lumens and that their fusion may not be as random as expected. This proof of concept provides hope of creating an interconnected vessel system that can be perfused while engineering large tissues in the future(Livoti and Morgan (2010)).

1.3.7 Honeycomb Microtissue Building Units

After the successful proof of concept that a toroid microtissue can function as a building block for larger tissues, the construction of honeycomb microtissues was studied (Livoti and Morgan (2010)). It had been shown that monodispersed cells are capable of forming complex shapes such as a honeycomb structure using micromolded non-adhesive agarose gels in previous experiments(Dean et al.

(2007)). Next, this self-assembly process was optimized by studying their formation and viability as building units for larger tissues when combined. It was observed that the rate of formation of honeycomb structures greatly depends on the properties of the individual cell types being seeding, Where more contractile cells are less successful in forming stable structures such as NHFs(Tejavibulya et al. (2011)).

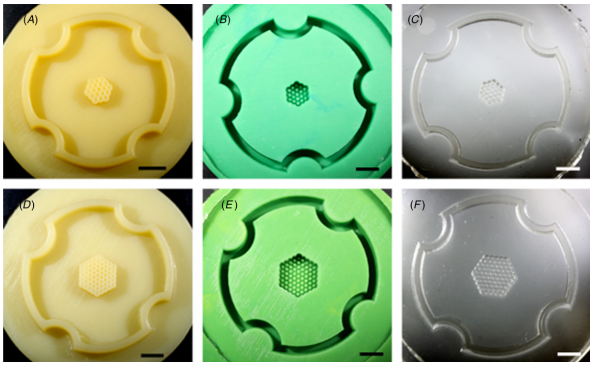

Figure 1.9: Wax replicates and two honeycomb mold designs used to make honeycomb microtissues((Napolitano et al., 2007))

The size of honeycombs based on orbitals was also studied, with the largest honeycomb structure containing eight orbitals and the smallest containing four ($1\,\mathrm{cm}$ - $2\,\mathrm{cm}$, $2x10^6$ - $7x10^6$ cells). Viability of the structures was studied by removing the microtissues from the molds and allowing the structures to undergo contraction. As expected, more contractile cell types reverted to a spheroid at a faster rate. More mature honeycombs contracted at a slower rate when compared to honeycombs that were not allowed to culture as long (Napolitano et al. (2007)).

The advantage of using a honeycomb structure over a toroid is that it contains more lumens needed to create larger viable tissues. By having a larger tissue, there are also difficulties such as controlling the mechanical strain on the tissue after formation. Similar to how toroids behaved, it was observed that some honeycomb structures broke under the strain of cell-cell interactions. By controlling the mechanical stress of a honeycomb microtissue, honeycombs could be used as building blocks for biofabrication of larger tissues (Napolitano et al. (2007)).

1.3.8 The Bio-Pick, Place, and Perfuse

Knowing that spheroids, toroids, and honeycombs can be fused and utilized as building blocks for larger tissues, the next challenge is optimizing this process in a timely manner to construct more extensive tissue architecture. In order to biofabricate larger tissues, an instrument called the Bio-Pick, Place, and Perfuse (Bio-P3) was invented (Fig. 1.10).

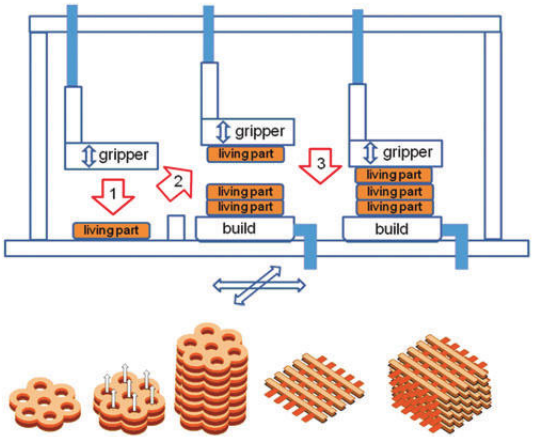

Figure 1.10: Diagram of Bio-Pick, Place, and Perfuse build box. (Blakely et al., 2015)

After self-assembly of microtissue units (spheroid, toroid, or honeycomb) in non-adhesive agarose gels, parts are removed from molds, transported to a build box, and constantly perfused with fresh media (Blakely et al. (2015)). Following being placed within the build box, a gripper that is connected to a peristaltic pump is able to pick up a microtissue, move it to a building platform and change flow direction to place the tissue accordingly on the platform (Fig. 1.11). By later adapting the Bio-P3 gripping mechanism to a fluid mechanics pump-driven grip, the amount force applied to pick up microtissues can be accurately quantified as well.

With this amount of control and high-throughput construction, the Bio-P3 can be used as a significant tool in the construction of tissues (Ip et al. (2016)).

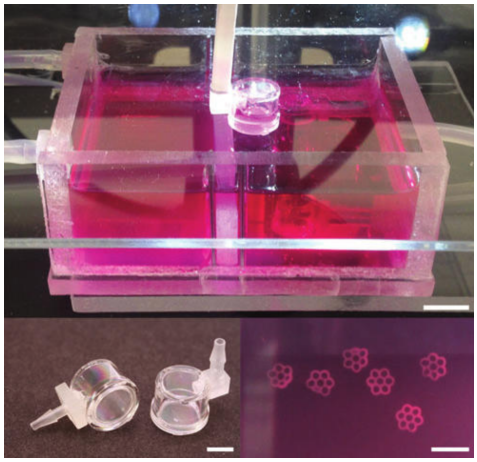

Figure 1.11: Image of Build Box and Gripper Head With Honeycomb Microtissues. (Blakely et al., 2015)

1.3.9 Incorporation of the Climbing Model and Bio-P3

With the invention of the Bio-Pick, Place and Perfuse, a step towards solid organ tissue engineering was taken. To test the ability of the Bio-P3, KGN toroids were created and stacked along a single capillary tube on the building platform (diameter approximately $100\,\mu m$) (Fig. 1.12). After 72 hours the toroids had completely fused around the capillary tube to form a tissue in the form of a tube.

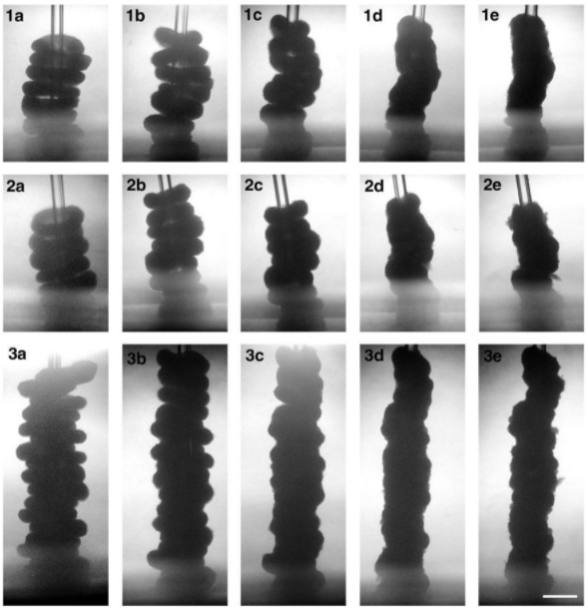

Figure 1.12: Image of toroid microtissue stacking using the Bio-P3. (Blakely et al., 2015)

As the Bio-P3 continues to be updated with new design features, a key component of the fabrication process is the timing of individual tissue formation

and specific geometrical features. As cells are seeded within different geometry molds, being able to predict when a tissue will be ready for removal from the mold is important. Having the flexibility to create different lumen diameter toroids could be vital for the design of vessels. As seen previously, when working with more contractile cell types, toroids will clearly contract at different rates. By having an accurate climbing model, it will increase the accuracy and pace of work flow as the system becomes more automated in the future.

1.3.10 Optimized Toroid Climbing Assay

Three-dimensional cell culture has been show to be more representative of *in vivo* structure. However, with this added dimension, the limits of traditional analysis techniques are pushed. This challenge lead to the creation of the toroid climbing assay in order to quantify cell power. Having this tool created a possible screening tool for three-dimensional cell culture. Continuing this work to provide a more high-throughput screening tool, this masters these will have three aims: (1) To redesign the non-adhesive agarose molds and verify the new geometries. (2) To track the changing toroid microtissue position on the mold ramp using a traditional bottom-view imaging process (3) To validate the bottom-view imaging process using side-view imaging.

Chapter 2

Materials and Methods

2.1 Normal Human Fibroblast Media Formulation and Cell Culture

Normal human dermal fibroblasts (NHF)(PromoCell) were grown and expanded in a solution of Dulbecco's Modified Eagle Media 1X (DMEM)(Gibco), 10% Fetal Bovine Serum (FBS)(Gibco), and 1% penicillin/streptomycin (P/S)(MP Biomedicals). Cells were kept in a sterile incubator at 10% carbon dioxide at $37°$C. Media was replaced every two days, or until the tissue culture flask was confluent. Upon flask confluence, cells were washed with PBS, trypsonized at a 0.05% concentration, and incubated for 5 minutes. After the short incubation period, the trypson solution was deactivated using serum free media. Cells were lightly agitated from the plastic surface and pipetted into a conical tube for counting and reseeding.For certain steps of passing cells and the entirety of the toroid climbing assay, a solution of serum free media plus collagen stimulating components (SFM[+]) was used. DMEM high glucose, sodium pyruvate, $50\,\mu\mathrm{g/mL}$ L-proline (Fisher Bioreagents), 0.1 mM L-ascorbic-2-phosphate trisodium salt (Sigma), and 1% P/S were filtered in a sterile environment and refrigerated until use.

2.2 3D Printing and Casting of Silicone Molds

Each mold iteration was designed using AutoDesk, edited in solidworks, and transferred to a 3D printer (Formlabs) in the form of an ASCII (.SAT) file. After the designs were printed using a proprietary plastic resin (Formlabs Clear Photopolymer Resin), molds were soaked in isopropyl alcohol for 10 minutes to remove excess resin. To further remove excess resin, an air brush was used to clean out the molds. The molds were then placed back into a second soaking period of 10 minutes. Molds were air brushed again and dried overnight before use.

Two part silicone rubber (Smooth-On, OOMOO 30) was created and then cast into the 3D printed plastic molds within a petri dish. To remove air bubbles from within the molds and allow the silicone to conform, the molds with the silicone mixture were placed in a vacuum. Air bubbles were removed for 3-5 minutes depending on the frequency of air bubbles being removed. Molds were then removed from the vacuum and silicone within the petri dish was added back to the molds. A second cycle was then used to removed air bubbles before the molds cured at room temperature overnight on a lab bench.Once the silicones molds had cured overnight, they were removed from the plastic molds and autoclaved.

2.3 Creation of Non-Adhesive Agarose Molds and Microtissue Formation

Non-adhesive agarose molds were created using the previously casted silicone molds. Agarose (Fisher Bioreagents) was sterilized by autoclave and dissolved in phosphate buffered saline (PBS)(Hyclone) by heating within a microwave to prepare a 2% w/v solution. Agarose was then pipetted into each mold and air bubbles were removed using a sterile spatula. To create a flat bottom surface, once air bubbles were removed from the mold a plastic microscope slide was placed on top of the mold. Gels sat for approximately 2 minutes before careful removal from the silicone mold. Each gel was then placed within a 24-well tissue culture plate. To hold each

Gel in place, $1\,\mathrm{mL}$ of agarose was pipetted into the base of each well and allowed to solidify. Gels were then equilibrated with SFM[+] for 24 hours. Juvenile normal human dermal fibroblasts (NHF) were trypsonized (cite), counted, and resuspended to the appropriate cell density necessary for seeding. Media was aspirated from the gels and 200,000 cells were then pipetted into the troughs of each non-adhesive agarose gel. After seeding, the 24-well plate was placed back in the incubator to allow the cells to settle into the trough of the gels. $2\,\mathrm{mL}$ of SFM[+] was carefully added to well and the plate was then placed within the wide-field microscope incubator for analysis of toroid formation.

2.4 Non-Adhesive Agarose Mold Design Validation

Accurate geometry of the non-adhesive agarose molds is an essential factor for the success of the assay. In order to validate the mold designs, each silicone mold was labeled after creation. Non-adhesive agarose molds were created from these labeled molds and placed into a 24-well plate. $1\,\mathrm{mL}$ of SFM[+] was added to each well and the gels equilibrated over night within an incubator.

Media was aspirated and the 24-well plate was removed from a sterile environment. The equilibrated gels were then removed from the 24-well plate and transferred to a square 8-well plate. Each gel was placed on its side, where the bottom side adhered to the wall of the square well plate. Next, PBS was added to each well until the peg of each gel was completely submerged. The plate was transferred to the stage of a Nikon Eclipse Ts2 Inverted Microscope. The images were taken using 2X objectives in order to examine the length and angle of the peg ramp. Images were exported and measured using ImageJ.

2.5 Toroid Climbing Imaging and Analysis

Wide-field Microscopy (Zeiss) in conjunction with Zen Blue 2.3 software (Zeiss) was used to collect bottom-view images of tissue formation and contraction

within the molds. Using a 2.5X objective, a 24-hour timelapse was conducted. Before imaging, toroids within a 24-well plate were brought into focus and centered. During imaging, 40 images were taken at increasing z-heights of $50\,\mu\mathrm{m}$ per time-point to capture the toroid microtissue in focus as it climbed the non-adhesive agarose mold. At the conclusion of the timelapse experiment, the 24-well plate was returned to the $37°$C, 10% CO_2 incubator.

2.6 Toroid Position Validation

When validating the position of a toroid microtissue within a non-adhesive agarose mold, the procedures for the creation of non-adhesive agarose molds and microtissue formation (2.3), mold design validation (2.4), and timelapse toroid microtissue imaging were combined (2.5). The only divergence from these procedures was that the 24-well plate was not placed within the wide-field microscope incubator for the entirety of the experiment and after 12 and 24 hours specific microtissues were fixed using 4% formalin. Following seeding of 200,000 NHF cells/toroid within non-adhesive agarose molds with ramp angles of $45°$ and $75°$, certain toroid contractions were interrupted using 4% formalin. $1\,\mathrm{mL}$ of 4% formalin was added to individual wells of the 24-well plate, where it was allowed to sit for 20 minutes before removing the original $1\,\mathrm{mL}$ of 4% formalin and a new $1\,\mathrm{mL}$ of 4% formalin was added and allowed to incubate for 24 hours. After 24 hours, the rest of the non-fixed toroids were interrupted using 4% formalin with the same procedure previously described. Microtissues were allowed to incubate within a $37°$C, 10% CO_2 incubator for 24-hours until 4% formalin was removed and replaced with PBS. Following removal of the fixative, bottom-view images were taken of each fixed toroid using the same wide-field microscopy procedure. Toroid microtissues were then immediately transfered to a square 8-well plate. The base of each non-adhesive agarose mold was carefully adhered to the vertical walls of the square well plate and molds were submerged in PBS. Side-view images were then taken using a Nikon Eclipse Ts2 Inverted Microscope. Bottom-view calculations were done using the Zen 2.3 software

and side-view calculations were conducted by ImageJ software.

Chapter 3

Mold Design Progression

3.1 Introduction

The toroid climbing assay was created in order to observe and quantify toroid microtissue contraction up defined mold geometries (Fig.3.1). As seen in previous experiments, the specific design elements of each mold plays a critical role in the self-assembly, quantification and contraction of the microtissue (Fig.1.4). By observing the changing inner lumen diameter of a toroid microtissue using wide-field microscopy, we hypothesize that the position of a toroid within a non-adhesive agarose mold at a specific time-point can be extrapolated if the specific geometries of the molds are known (Fig.3.2).

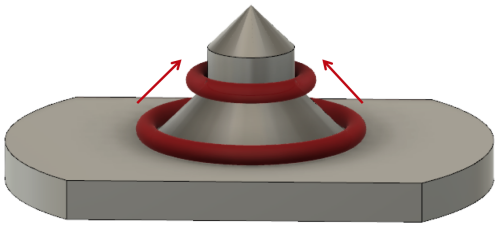

Figure 3.1: 3D rendering of toroid microtissue using centripetal contraction to move up angled non-adhesive agarose ramp. Toroids will then contract around a central peg at the top of the ramp, preventing it from leaving the mold.

Previous mold designs used for side-view toroid climbing had ramp angles of $55°$, $65°$, and $85°$ (Fig. 1.7). The purpose of the increasing angle steepness was to incrementally raise the amount of gravitational force that the toroids had to

work against to climb the agarose pegs (Youssef et al. (2011)). For the design of an optimized climbing assay, the same general conception was used in 15% increments. Angles experimented with consisted of $45°$ and $75°$ molds. $30°$, $60°$ and $90°$ degree angle molds were created, but not used in testing.

Each mold needed to have a long enough ramp to capture the entirety of the self-assembly and stages of contraction of the microtissue. To maintain consistency between different mold angles, each mold had a ramp length of $1\,\mathrm{mm}$. We believed that by having an invariable ramp length, comparison between different molds would be more straightforward. With having an unchanging ramp length, but a varying ramp angle, the only differences between each mold is the final central peg diameter at the top of the ramp. Every mold ramp started with the same base diameter of $2.5\,\mathrm{mm}$. The $45°$ and $75°$ molds result in final toroid lumen diameters of $1.1\,\mathrm{mm}$ and $2.0\,\mathrm{mm}$ accordingly.

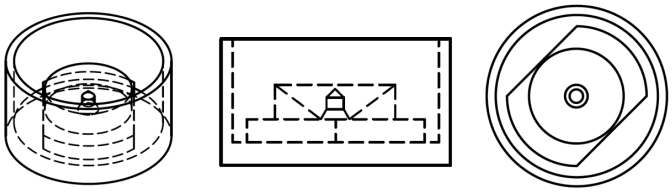

Figure 3.2: 3D sketches of non-adhesive agarose mold

A major limitation of the side-view molds was the loss of microtissues from the pegs after a certain time period. Toroids would contract and pop off of the agarose peg and further contract to spheroids. This limited the assay from conducting any endpoint experiments and continued toroid testing. In order to resolve this, at the top of the $1\,\mathrm{mm}$ ramp a $90°$ central angle peg was added. The peg extruded roughly $1.5\,\mathrm{mm}$ vertical and was beveled to create a peak.The peak prevented cells from aggregating on the top of the peg when seeding, and promoted cells to settle within the trough (Fig.3.3).

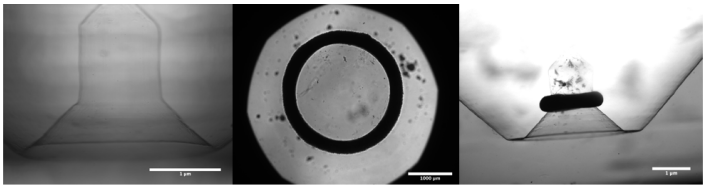

Figure 3.3: Addition of central peg at top of ramp prevented toroid microtissues from contracting off of mold.

3.2 Mold Design One

The first series of molds experimented with the idea of not having a flat-bottom trough for cells to settle into. From past experiments it was established that flat bottom molds could result in satellite spheroids that never conform with a full toroid tissue (Fig.1.4). Satellite spheroids are cells that do not aggregate with the toroid, instead forming small spheroids within the trough. It was also shown that a round bottom trough could improve the self-assembly of tissues(Fig.1.4). Working off of this, the first series of molds would have wells that would connect directly to the base of the ramp (Fig. 3.4).

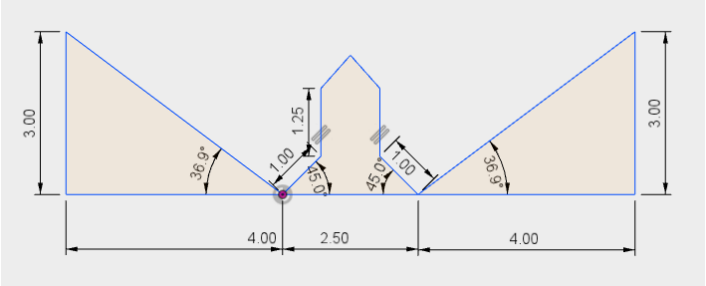

Figure 3.4: First iteration of toroid climbing molds with $45°$ ramp. As shown above, the ramp connects directly to the well

The main goal of this modification was to see if having a similar concept as a round bottom trough promoted tissue formation. The future intention of this design was to observe formation of toroid microtissues at decreasing cell seeding densities. In theory, cells would settle closely together in a more compact environment without a flat bottom trough, possibly being able to create stable toroid microtissues at lower seeding densities.

3.3 Mold Design Two

For the second iteration of molds there were two major changes. After experimenting with the first series of molds, changes to the trough and well angle needed to be made. It was observed that the first molds did not have a steep enough well angle to prevent the cells from settling on the well instead of in the trough. Therefore, the angle of the well was raised from $36.9°$ to $45°$. With this increase in well angle to $45°$ came the question of toroid morphology during formation.

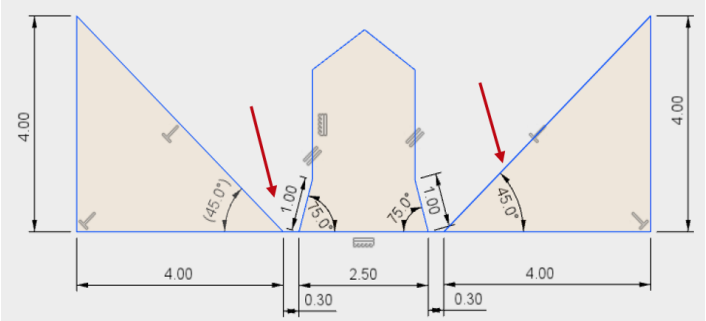

Figure 3.5: Second iteration $75°$ ramp mold

As the well angle increases, the formation that the toroid tissue would initially be exposed to upon seeding would be restricted. In order to counter this, a $300\,\mu m$ trough connecting the ramp and the well was added. Another reason to add the trough was based on the observation that after seeding, cells would widely collect directly on the ramp and not at the base. With this, toroids would form, and begin contracting at different starting points on the ramp. Ideally, cells would gather in the new trough, form toroids, and being contracting from the same initial starting point.

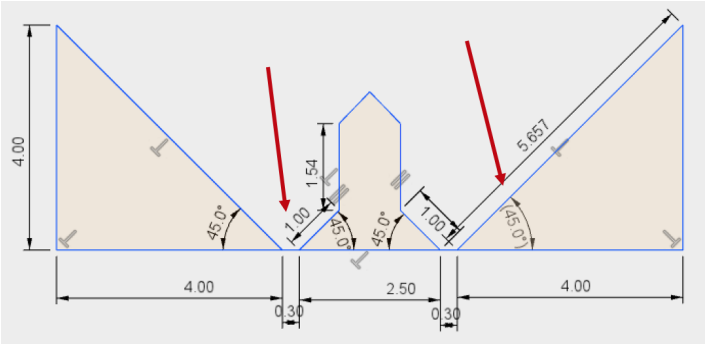

Figure 3.6: Second Iteration $45°$ ramp mold.

3.4 Mold Design Three

Lastly, the 3rd iteration of molds was created with only one change. After increasing the well angle to $45°$ for the second iteration, cells were not collecting on the well. However, cells were still sitting on the ramp and not completely in the trough for the $45°$ angle molds. This could partly be due to the lack of 3D printing accuracy below $500\,\mu m$. To resolve this, the trough diameter was increased from $300\,\mu m$ to $500\,\mu m$.

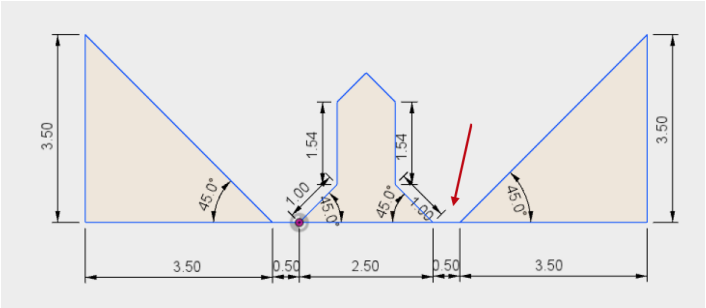

Figure 3.7: Third iteration $45°$ ramp mold.

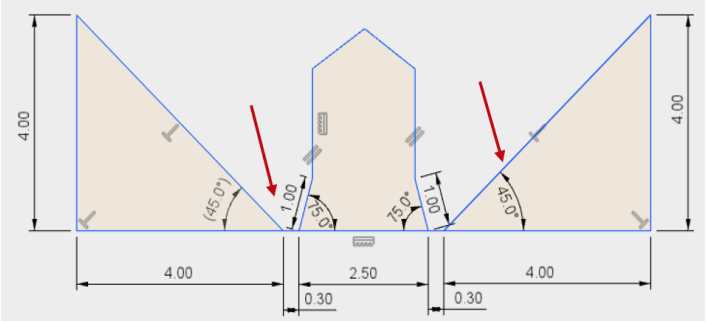

Figure 3.8: Third iteration $75°$ ramp mold.

With this alteration, cells started completely off of the ramps of the molds. Toroids would then begin to consolidate into a more defined tissue within the trough and then contract up the ramp, contrary to previous mold iterations where often the tissues would form while on the ramp. A toroid initially starting at the base of the ramp is important in order to see the complete process of the tissue contracting up the ramp. The main downside to the $500\,\mu m$ diameter trough is seeding within the molds can be somewhat troublesome. Users must be cautious to seed cells completely around the trough and not to just one side, otherwise an incomplete toroid will form.

3.5 Verifying Mold Geometries

Knowing the dimensions of the molds greatly influences accurate interpretations of the lumen diameters. In order to validate the non-adhesive agarose mold geometries created initially from the 3D printed plastic molds, multiple agarose molds needed to be measured using side-view microscopy. For each iteration, a specific amount of molds were made as if they were going to be used to form toroid microtissues. These molds were equilibrated overnight in SFM+, then removed and placed in a square well plate with PBS. Each gel was placed on its side and the base adhered to the side of the square well plate. Gels were then entirely submerged in PBS and imaged at a 2X objective.

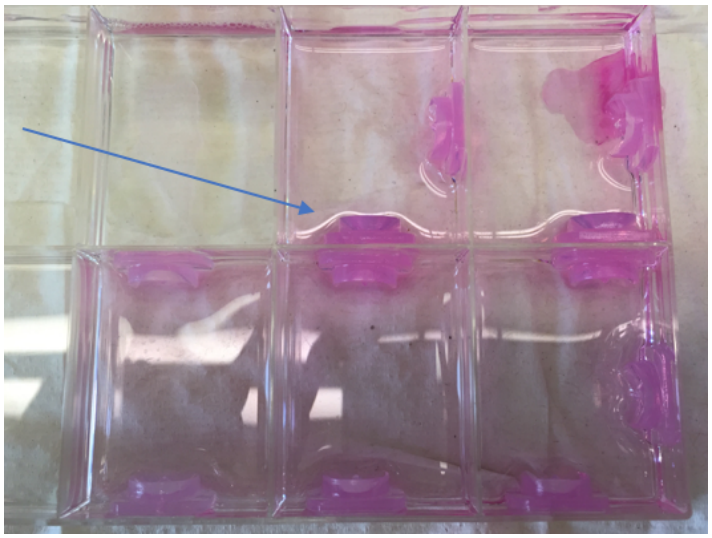

Figure 3.9: Method to Collect Side-View Images: In order to collect side-view images of non-adhesive agarose molds, molds were incubated in DMEM, and the bottom of each mold adhered to a square well plate. PBS was then added to the wells to submerge the molds.

The base of each ramp within a mold was identified and a line was drawn to the top of the ramp where the peg extended $90°$. That same ramp line was then used to measure the angle of the ramp across to the opposite side (Fig. 3.10) . For the $45°$ ramp molds the average ramp angle was $43.56°$ +/- $1.12°$ and the ramp length average was 980.0 um +/- 3.00 um (N_{Molds} = 10). $75°$ molds had an average ramp length of 1006 um +/- 13.98 um. The average $75°$ mold ramp angle was $73.87°$ +/- $0.66°$ (N_{Molds} = 10)(Fig.3.11).

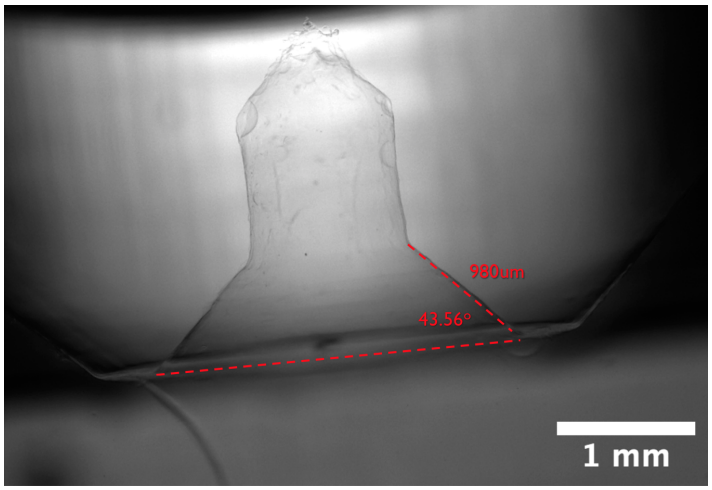

Figure 3.10: Side-view Image With Geometry Measurements for $45°$ Ramp Mold.

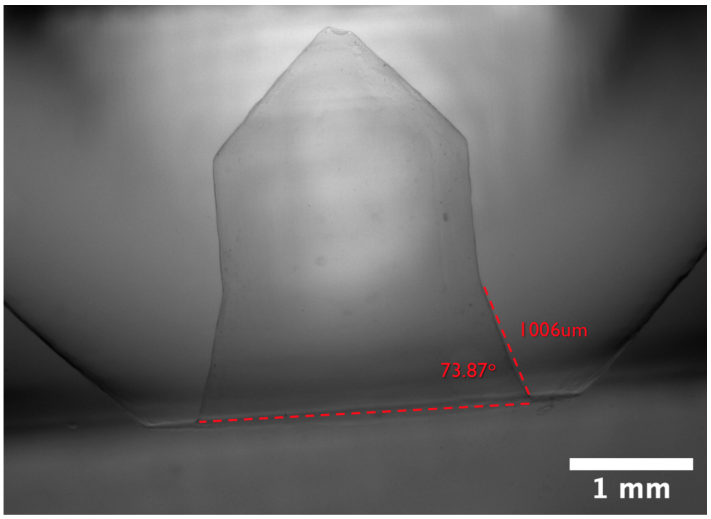

Figure 3.11: Side-View Image With Geometry Measurements for $75°$ Ramp Mold.

Chapter 4

Toroid Climbing Assay

4.1 Results

The toroid climbing assay was optimized to provide a more rapid way to observe and quantify toroid microtissue contraction for the purposes of biofabrication and mechanobiology. Using bottom-view, wide-field microscopy, cells seeded into gels of specific geometries will self-assemble into toroid microtissues and begin to contract up a ramp over time. The tissues will then reach the top of the ramp and remain constrained to an agarose peg. In this proof of concept experiment, NHF toroids were created within gels and the changing inner lumen diameters were recorded. The diameters were then used to deduce the approximate position of the tissues within the gel.

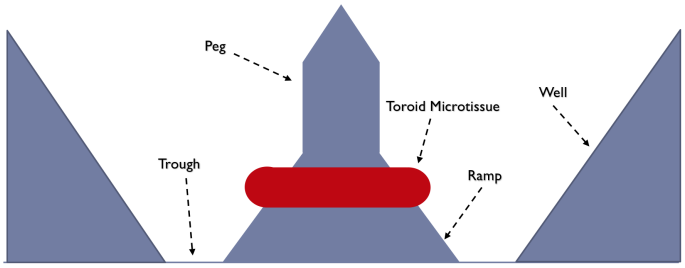

Figure 4.1: Anatomy of a non-adhesive agarose mold: Cells are seeded into the trough, where the toroid microtissue self-assembles and begins to climb the ramp.

4.1.1 Calculations

Ensuing the collection and organization of bottom-view images of the toroid microtissues, the inner lumen areas were calculated using Zen 2.3. In order to calculate the diameter of the lumen area, it was assumed that the region was a perfect circle. Using formula (Equation 4.1), the inner lumen diameter was calculated.

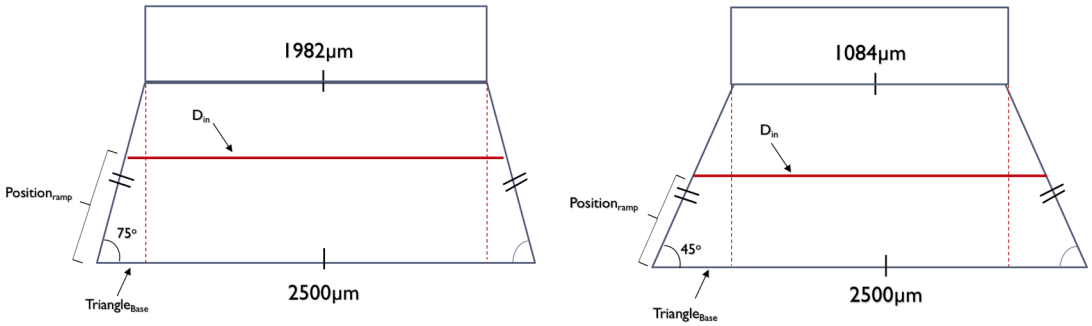

Figure 4.2: Diagram of $45°$ and $75°$ molds and how position was calculated. Using the diameter (D_{in}), the triangle base ($triangle_{Base}$) of the angled ramp was calculated. From the $triangle_{Base}$, the cosine of whatever angled mold is being used results in the ramp position.

$$D_{in} = 2 * \sqrt{\frac{A_{lumen}}{\pi}} \tag{4.1}$$

Using the inner lumen diameter and based on the specific mold geometry, the base of the ramp length is calculated ($Triangle_{Base}$) (4.2). Knowing that the entire base of the gel ramp is $2500\,\mu m$ total, D_{in} can be subtracted and divided by two to reach $Triangle_{Base}$ (4.2).

$$Triangle_{Base} = \frac{(2500\,\mu m - D_{in})}{2} \tag{4.2}$$

From $Triangle_{Base}$ the position or distance up the ramp the toroid has traveled is calculated as $Position_{Ramp}$. By dividing the previously calculated $Triangle_{Base}$ by Cosine of $45°$ or $75°$ depending which mold is being used, the toroid position on the ramp can be calculated (4.3).

$$Position_{Ramp} = \frac{Triangle_{Base}}{\cos 45^\circ} \tag{4.3}$$

In order to calculate the change in toroid thickness the same process of finding the inner lumen area was applied to the entire toroid including the lumen. From the bottom-view, the entire toroid area along the inner lumen area was measured and diameter ($D_{Microtissue}$) was calculated using equation 4.1. Having previously calculated the inner lumen diameter (D_{in}) of the microtissue, the lumen diameter was subtracted from the the entire microtissue including inner lumen area diameter (4.4). This resulted in the toroid thickness or diameter alone (Fig.4.2).

$$Thickness = \frac{D_{Microtissue} - D_{in}}{2} \tag{4.4}$$

4.1.2 Toroid Microtissue Climbing of Mold Design One

The first iteration of molds did not consist of a trough and only 45° molds were made (Fig.3.4). 200,000 NHF cells were seeded into each individual mold and allowed to stabilize for 20 minutes before beginning the imaging process. Once imaging began, toroid microtissues continued self-assembly and contracted up the ramp at an initial ramp starting position of $200\,\mu\mathrm{m}$. The average NHF toroid microtissue reached the top of the ramp at 8 hours +/- 30 min (Fig.4.3) .

4.1.3 Z-stack Comparison

With microtissues climbing the mold ramp, their z-depth while being imaged is constantly changing. In order to capture the microtissue in focus at its specific z-position, a z-depth range was used while imaging. Following the first pilot run of the optimization of the toroid climbing assay with the first iteration molds, we identified the appropriate z-range needed to be for future trials (Fig.4.4). Along with assessing the range, lumen area measurements were compared at varying z-depths for a single position to see the sensitivity of z-depth accuracy on calculations (Fig.4.5).

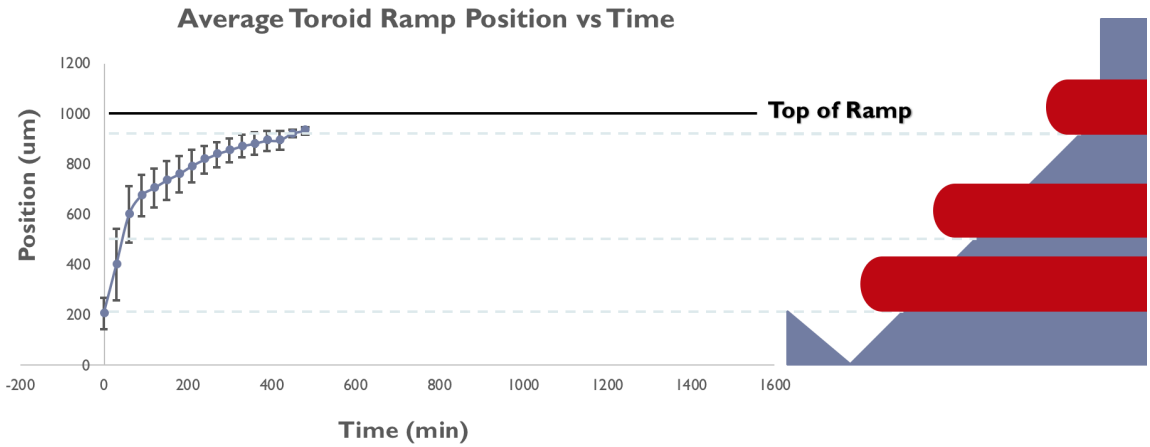

Figure 4.3: NHF Toroid Climbing $45°$ First Iteration Molds. The positions of the toroid microtissues were tracked over time within the non-adhesive agarose gel. The Schematic is a relative side-view approximation of actual toroid position on the ramp.($N_{Toroids}$ = 5)

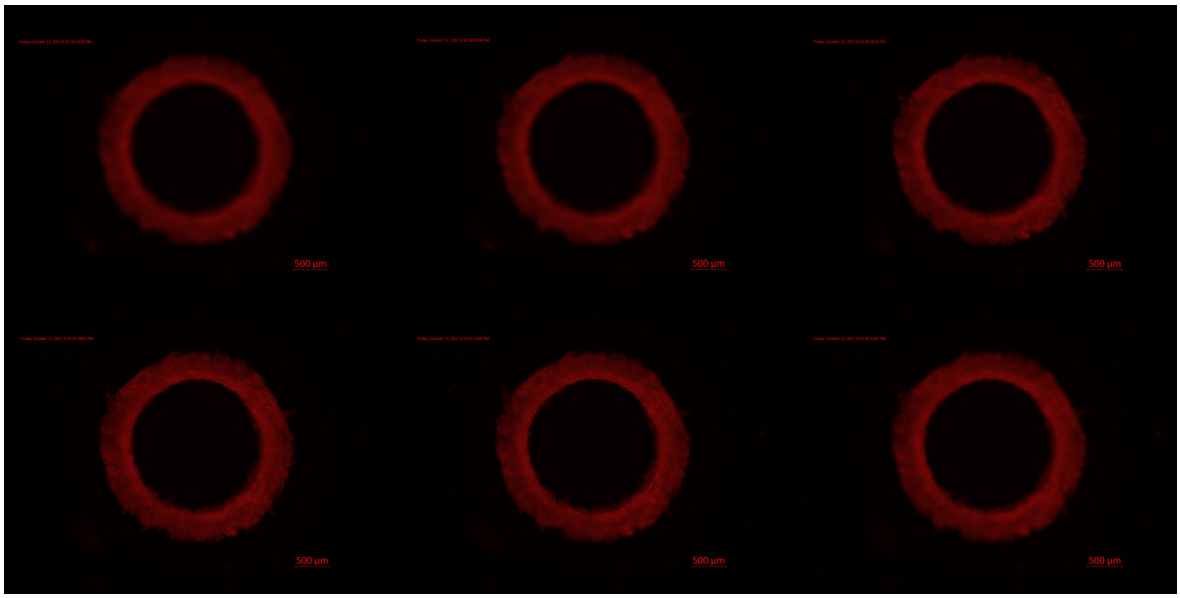

Figure 4.4: Comparison of single tissue at incrementally increasing z-positions of $50\,\mu m$ (Starting with top moving left to right, increasing with z-height).

4.1.4 Toroid Microtissue Climbing of Mold Design Two

Following trials with the first iteration of molds, design changes were made for the second iteration. A $300\,\mu m$ trough was added and the well angle was increased to $45°$. In addition to the $45°$ ramp mold, a second $75°$ ramp mold was introduced (Fig.3.6, Fig.3.5). Similar to the first iteration experiments, 200,000 NHF

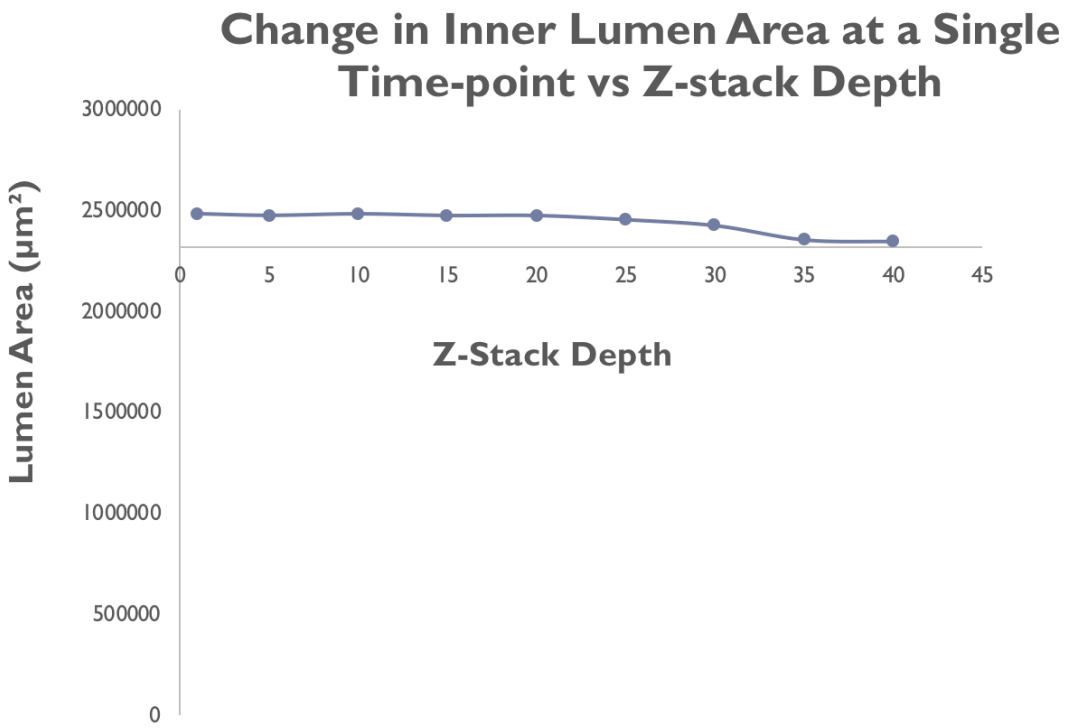

Figure 4.5: Measurement of inner lumen area for an individual toroid microtissue at $50\,\mu\mathrm{m}$ incremental z-height positions (1-40).

cells were seeded into each individual mold. Subsequently, toroid microtissues self-assembled and began to contract up the non-adhesive agarose mold ramp at varying rates. These varying climbing rates were dependent on either the $45°$ or $75°$ ramp molds used.

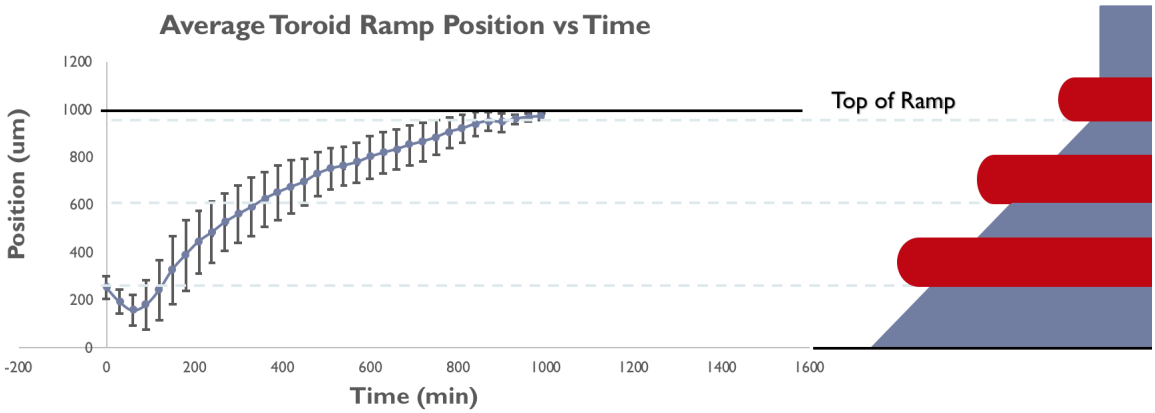

Figure 4.6: NHF toroids climbing $45°$ second iteration molds with $300\,\mu\mathrm{m}$ trough ($N_{Toroids}$ = 5).

For the second iteration $45°$ ramp molds, toroids initially started to form

at roughly 200 µm and descended to completely self-assemble at 150 µm where they later continuously contracted up the ramp. Toroids reached close to the top of the ramp (1000 µm) at approximately 16.5 hours +/- 30 minutes. It can be seen that toroids ascended at steady rate that began to plateau as they approached the top of the ramp (Fig.4.6). For the new second iteration 75° ramp molds, toroids began to form within the trough before ascending the ramp after 3 hours. Once climbing began, toroids moved 200 µm up the ramp then stalled for 3 hours before advancing up the ramp to 700 µm. At this point from a bottom-view perspective it appeared that toroids had reached the top of the ramp (Fig. 4.7).

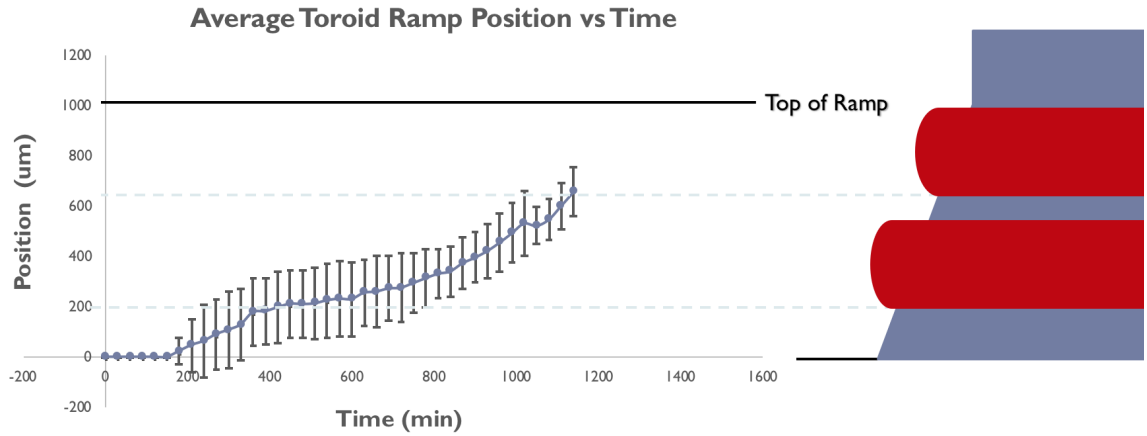

Figure 4.7: NHF toroids climbing 75° second iteration molds with 300 µm trough ($N_{Toroids}$ = 5).

4.1.5 Toroid Microtissue Climbing of Mold Design Three

The third iteration contained 45° and 75° ramp molds (Fig.3.7, Fig. 3.8). The only modification made to the third iteration in comparison to the second iteration molds was the increase of the trough diameter from 300 µm to 500 µm. Toroids were seeded at the same seeding density of 200,000 NHF cells/toroid. After an incubation period that allowed the cells to become stabilized, images were collected. The changing inner lumen area over time was tracked, which was later used to calculate the toroid lumen diameter (Equation 4.1). The change in inner lumen diameter was graphed over time (Fig 4.8). Based on the inner lumen diameter, toroid ramp position was extrapolated using the specific mold geometries (Equations 4.2 and 4.2).

For the $45°$ molds it was observed that toroids began formation around the $150\,\mu m$ position on the ramp and descended to near the base of the ramp to further assemble at the $50\,\mu m$ to $100\,\mu m$ position (Fig. 4.9). Followed by the initial assembly and rapid contraction of the toroid, it was observed that the toroids stalled between the $400\,\mu m$ to $600\,\mu m$ position on the ramp. This stall or slow contraction phase lasted for roughly 4 hours before the rate of climbing increased to the top of the ramp. The average total climbing time to the top of the ramp for the $45°$ ramp molds was 19.5 hours +/-30 minutes. It was observed that after seeding, toroids in the $45°$ mold underwent a change in thickness (Fig. 4.4). Starting at an average thickness of $2049\,\mu m$, thickness exponentially decreased to $780\,\mu m$ around 600 minutes. After 600 minutes, thickness did not drastically change, ending with a final thickness of $750\,\mu m$ when the microtissue reached the top of the ramp.

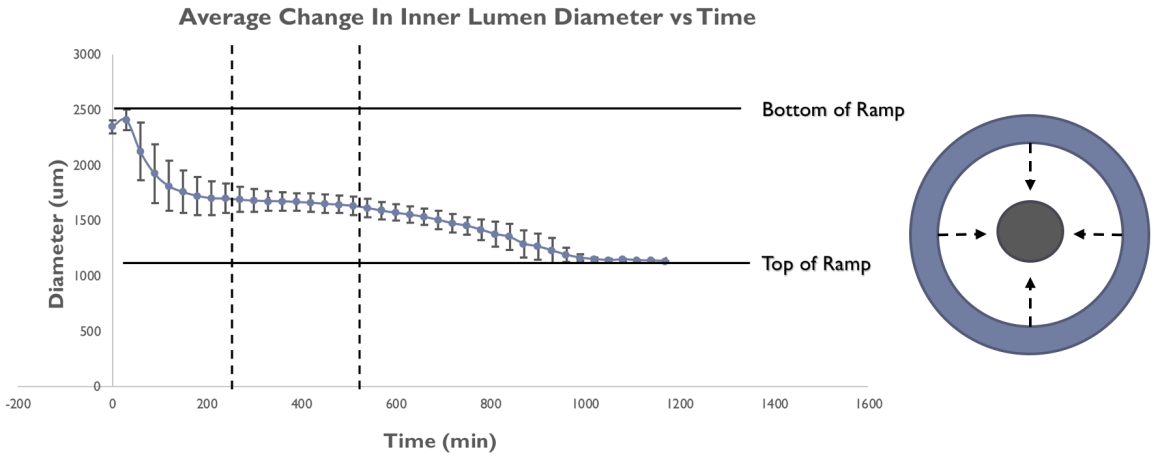

Figure 4.8: Average change in inner lumen diameter over time for the third iteration $45°$ mold. Vertical dotted lines indicate a period of stalling while contracting up the mold ramp ($N_{Toroids}$ = 8).

Adjacent to the $45°$ ramp molds, $75°$ ramp molds were placed in the same plates to be simultaneously tested for the third iteration. Toroids were seeded at the same 200,000 NHF cells/toroid as the $45°$ ramp molds in the plate. Thereafter, toroids began to self-assemble within the troughs of the molds before ascending up the ramp. Like previous iterations, the inner lumen diameter was tracked over time using equation 4.1 (Fig. 4.11). From these diameter calculations, using equations

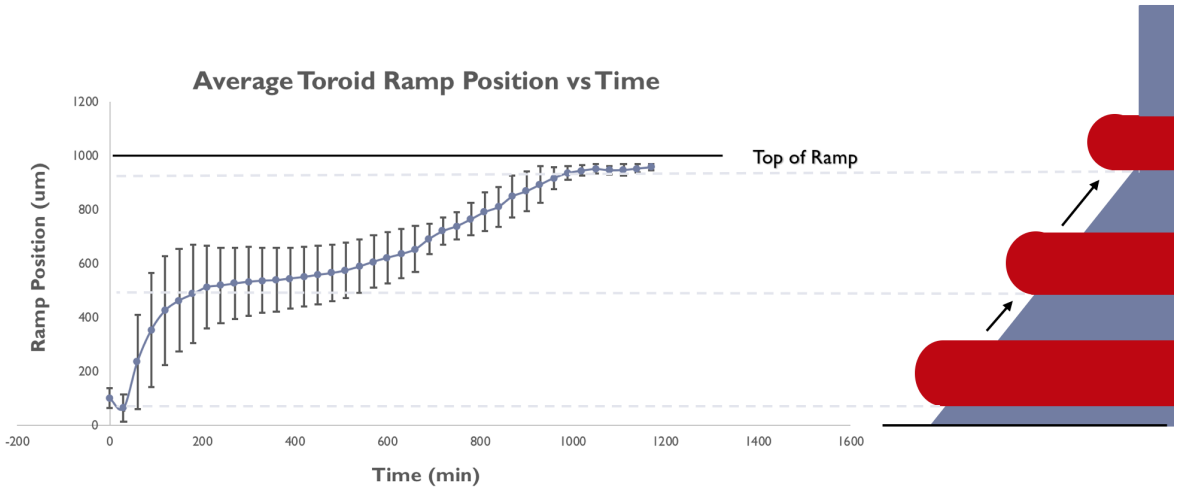

Figure 4.9: NHF toroids climbing $45°$ third iteration gels with $500\,\mu m$ trough ($N_{Toroids}$ = 8). The diagram to the right of the graph is a hypothetical model of tissue position from a side-view.

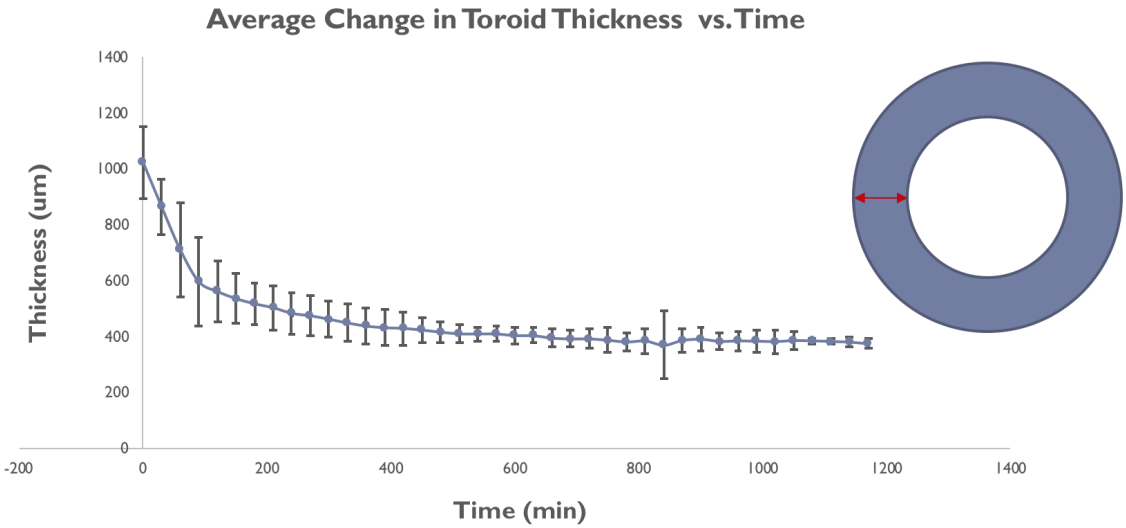

Figure 4.10: Average change in toroid thickness over time for $45°$ toroid microtissues. Final thicknesses were roughly $750\,\mu m$ ($N_{Toroids}$ = 5).

4.2 and 4.2, the toroid position on the ramp was deduced. The ramp position over time was graphed, showing that toroid microtissues self-assembled first entirely in the trough. ($Position_{Ramp} = 0\,\mu m$) (Fig. 4.12). Toroids began to climb the ramp after 30 to 60 minutes, where they reached a position of $150\,\mu m$ to $250\,\mu m$ on the ramp before stalling. This stalling or slow contraction phase lasted for approximately 12 hours +/- 30 minutes. After, toroids contracted up the ramp at an exponential rate to a final position of $750\,\mu m$. The total climbing process took roughly 23 hours +/-

30 minutes. As stated before, until validated it is assumed that the base of the tissue is being viewed while climbing and that the toroids reached the top of the mold with the bottom of the microtissues resting near $750\,\mu m$ for the 75° molds (Fig. 4.12). Toroid thickness was calculated by subtracting the lumen diameter from the entire toroid diameter including lumen diameter. This toroid thickness was then tracked over time, showing an exponential decrease. The 75° toroid microtissues appeared to plateau in thickness at $525\,\mu m$ while climbing, ending with an average thickness of $540\,\mu m$.

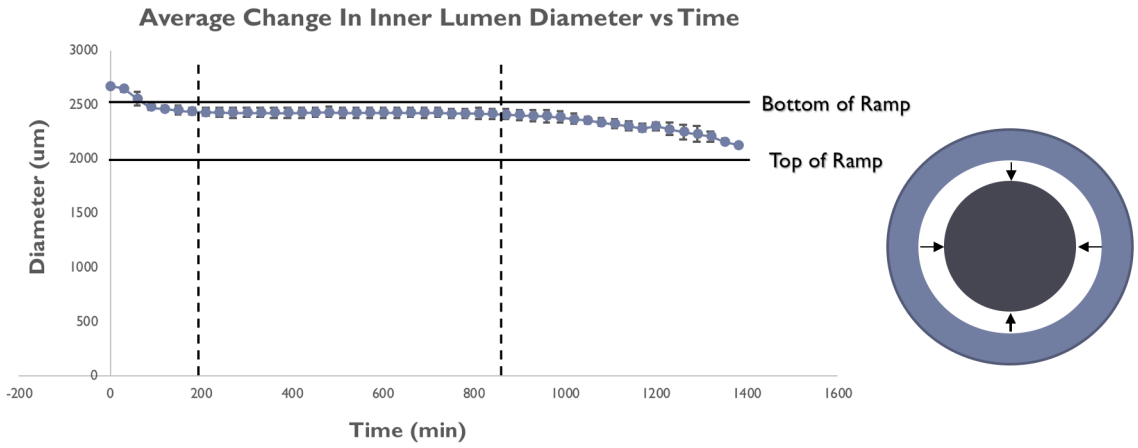

Figure 4.11: Graph of the changing inner lumen diameter over time for the 75° mold. Vertical dotted lines indicate a defined stalling phase while climbing the mold ramp ($N_{Toroids}$ = 8).

In order to give an in-depth comparison of the 45° and 75° toroids climbing over time during the third iteration, both position graphs were overlapped (Fig. 4.14). Here it can clearly be seen that the 45° microtissues climbed to a higher base position than the 75° microtissues. The 45° microtissues were also able to climb the ramp at a faster rate than the 75° microtissues. In order to understand the discrepancy between the final 45° and 75° microtissue positions, after 24 hours side-view images were taken of both angled molds to understand the final resting position (Fig. 4.15).

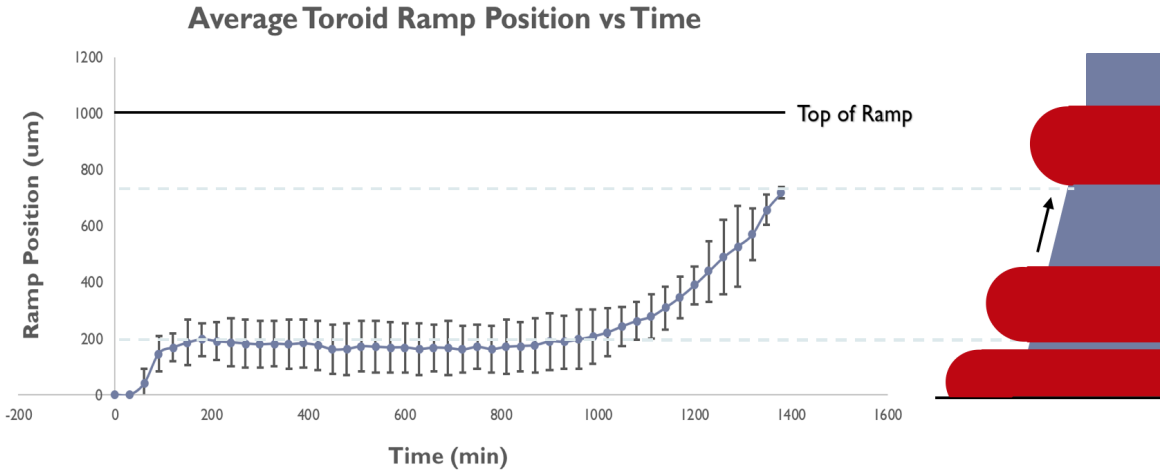

Figure 4.12: NHF toroids climbing $75°$ third iteration molds with $500\,\mu m$ trough ($N_{Toroids}$ = 8). The diagram on the right is a hypothetical side-view model of microtissue position.

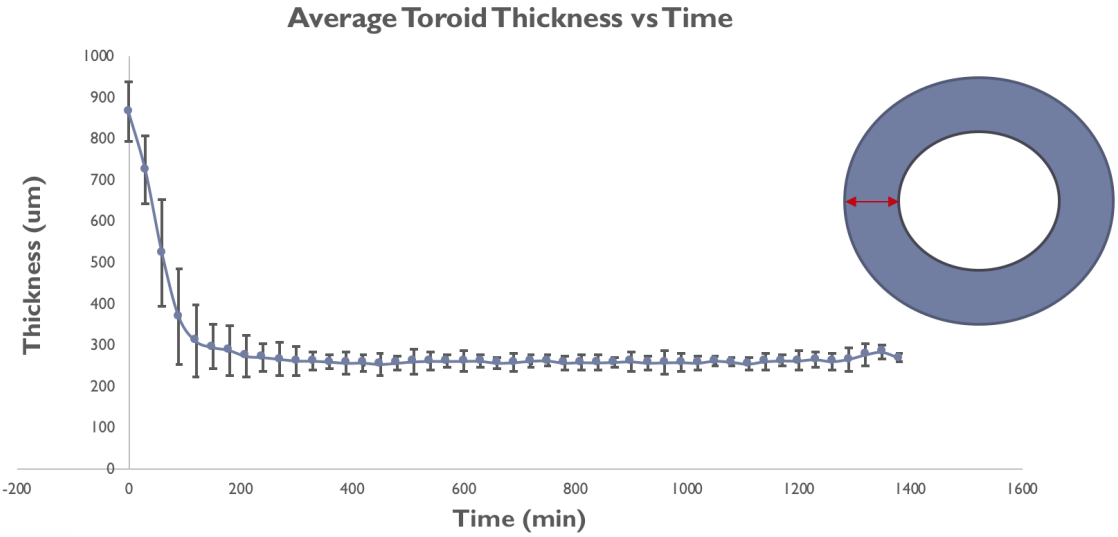

Figure 4.13: Average change in toroid thickness over time for $75°$ toroid microtissues in $500\,\mu m$ mold. Final thicknesses were approximately $540\,\mu m$.

4.1.6 Toroid Climbing Validation

A consequence of using bottom-view microscopy was not knowing the actual resting position of the microtissues at the tops of the ramps for the $45°$ and $75°$ ramp molds for the third iteration until validation. In order to validate this process, the identical procedure for the third iteration climbing experiment was conducted with the addition of side-view. At 12 hours, climbing was interrupted for specific

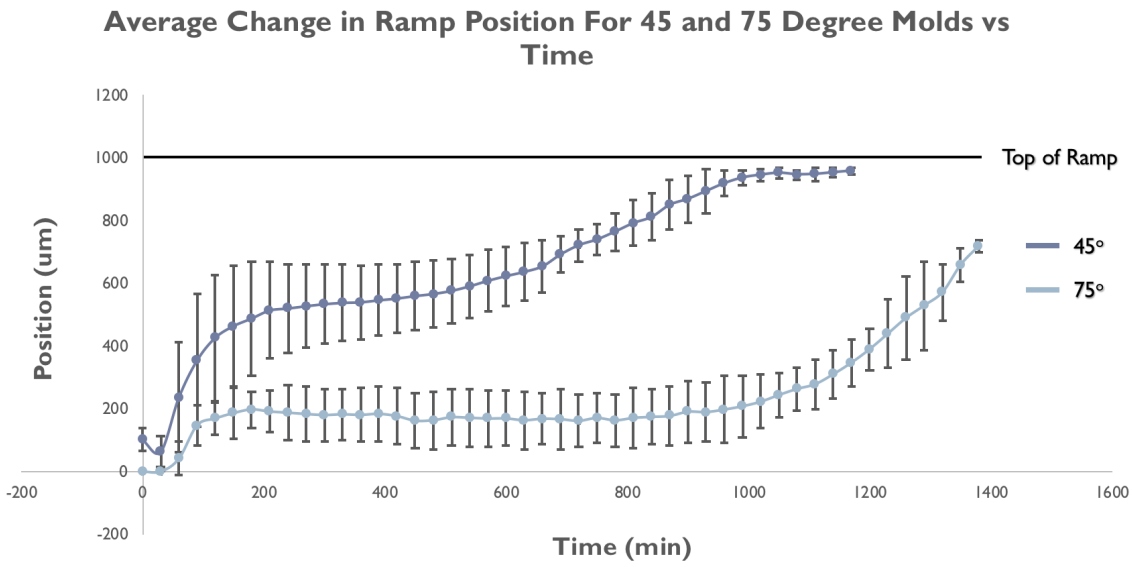

Figure 4.14: Overlapped graphs of the $45°$ and $75°$ mold ramp positions ($N_{Toroids}$ = 5).

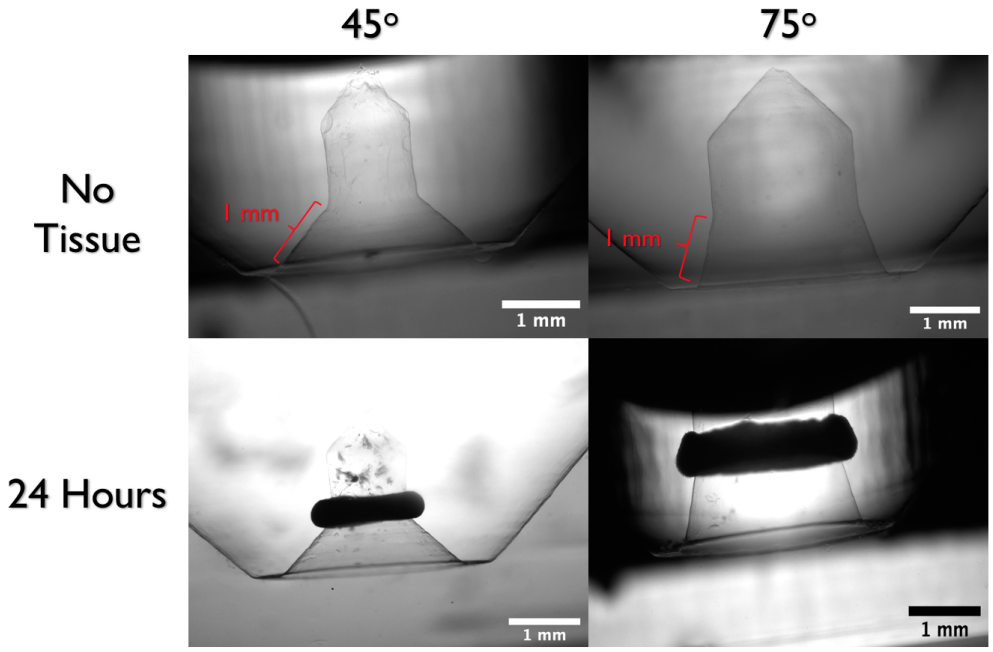

Figure 4.15: Side-view images of the third iteration $45°$ and $75°$ molds. The top row does not contain a toroid microtissue. The bottom row contains side-view images of toroid microtissues after 24 hours seeded within the $45°$ and $75°$ molds.

toroids within the $45°$ and $75°$ ramp molds by fixation with 4% formalin. A second round of toroids within the same plate for the $45°$ and $75°$ ramp molds were interrupted at 24 hours by fixation with 4% formalin. Ensuing fixation of the microtissues, bottom-view and side-view images for each toroid was taken (Fig. 4.15).

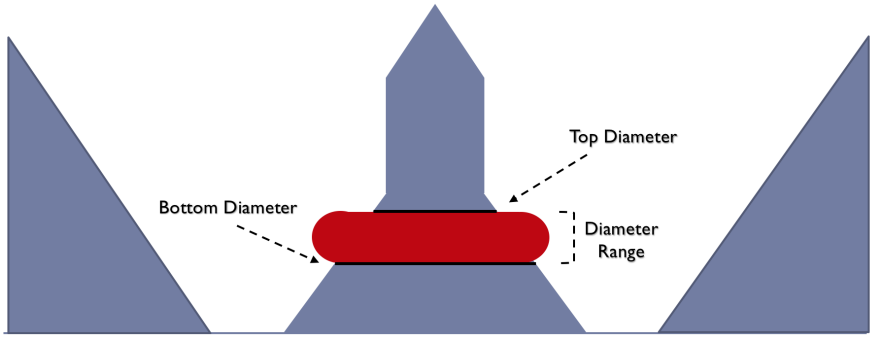

Figure 4.16: Diagram of how side-view toroid microtissue diameter range was calculated.

Using the same technique to collect the diameters of the past bottom-view diameters, diameters of the fixed toroid microtissues from a bottom-view were measured. Using ImageJ, the bottom and top diameters of the same toroids were measured from a side-view. Applying the top and bottom diameters, a diameter range of the tissue was generated (Fig. 4.16). This side-view diameter range was then used to validate the calculated diameter from bottom-view.

Table 4.1: $45°$ Third Iteration Mold Climbing Validation

Toroid	**Bottom View**	**Side-View**			
12 Hours	Diameter (um)	Diameter (Bottom) (um)	Diameter (Top) (um)	Diameter Range (um)	Is Bottom View Within Side View Range?
1	1248	1773	1104	1773 - 1104	Yes
2	1219	**Popped off peg**	-	-	N/A
3	1328	1466	1090	1466 - 1090	Yes
4	1196	1208	1089	1208 - 1089	Yes
Toroid	**Bottom View**	**Side-View**			
24 Hours	Diameter (um)	Diameter (Bottom) (um)	Diameter (Top) (um)	Diameter Range (um)	Is Bottom View Within Side View Range?
1	1408	**Popped off peg**	-	-	N/A
2	1164	1281	1084	1281 - 1084	Yes
3	1145	1407	1084	1407 - 1084	Yes
4	1147	1322	1084	1322 - 1084	Yes
5	1221	1278	1084	1278 - 1084	Yes
6	1176	1232	1084	1232 - 1084	Yes
7	1160	1218	1084	1218 - 1084	Yes

As seen in Table 4.1, the $45°$ bottom-view ramp mold diameters all coincided within the bottom-view diameter range. Popped off peg indicates that following bottom-view imaging, the toroids popped off the peg or drastically shifted while being moved to side-view imaging. To further validate the process, the average bottom side-view diameter after 24 hours was used to calculate $Position_{Ramp}$

(Equation 4.2) which was $838\,\mu m$, indicating that after 24 hours the bottoms of the toroids rest slightly below the top of the ramp ($1000\,\mu m$).

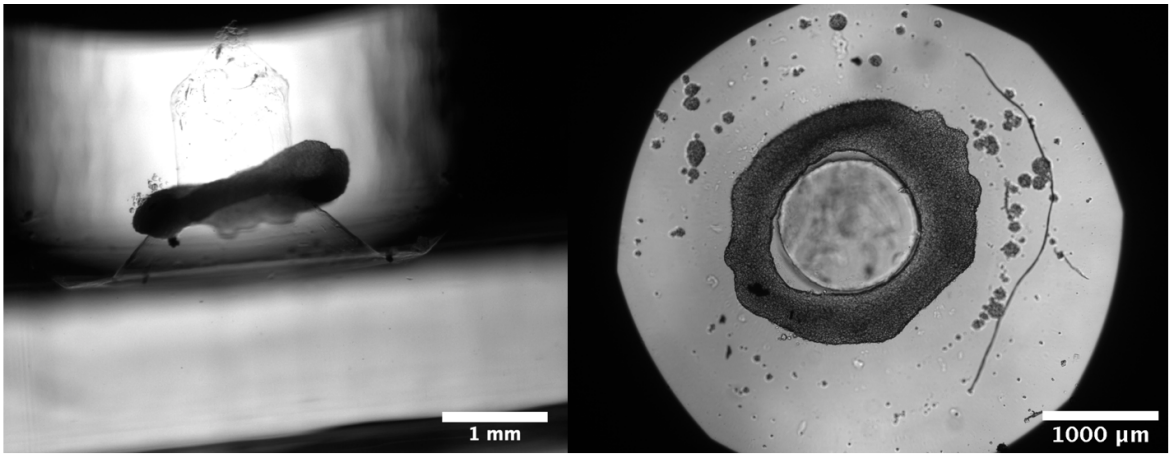

Figure 4.17: Side-view and bottom-view images of the same fixed tissue after 12 hours of contraction within $45°$ mold.

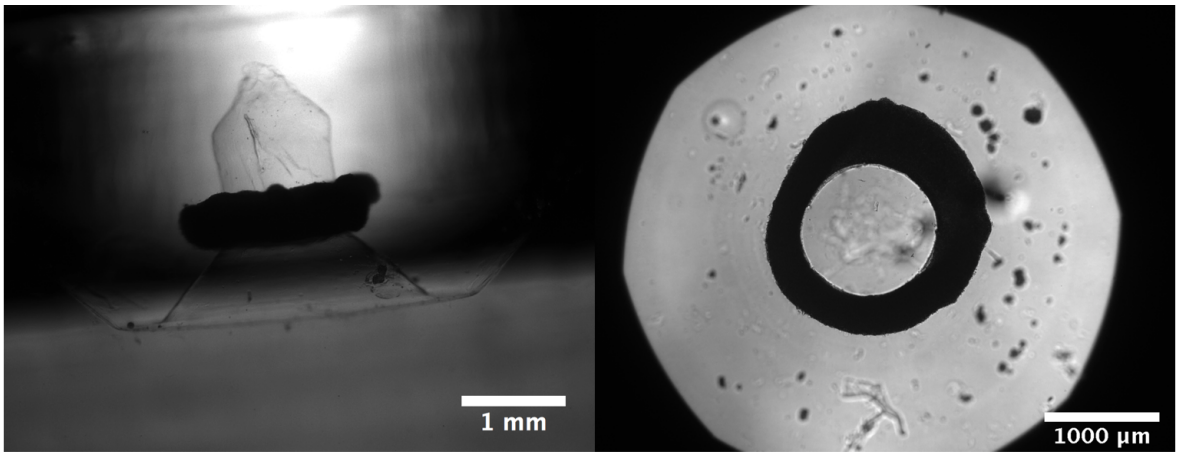

Figure 4.18: Side-view and bottom-view images of the same fixed tissue after 24 hours of contraction within $45°$ mold.

Table 4.2 represents the validation process of the third iteration $75°$ ramp molds. All 12 hour bottom-view toroid diameters coincided within the side-view diameter range. However, one toroid 24 hour bottom-view diameter did not coincide within its respective range. This microtissue bottom-view diameter was outside the side-view diameter range by $5\,\mu m$. To supplement the validation of the toroid positions at the top of the $75°$ ramp molds, the $Position_{Ramp}$ for the 24 hour fixed tissues was calculated using the average side-view bottom diameter (Fig. 4.2) . The average ramp position for the bottom of the side-view toroid microtissues was $701\,\mu m$.

Table 4.2: 75° Third Iteration Mold Climbing Validation

Toroid	**Bottom View**	**Side-View**			
12 Hours	Diameter (um)	Diameter (Bottom) (um)	Diameter (Top) (um)	Diameter Range (um)	Is Bottom View Within Side View Range?
1	2276	2358	1982	2358 - 1982	Yes
2	2153	2485	2188	2485 - 2188	Yes
3	2193	2343	2054	2343 - 2054	Yes
4	2311	2423	2135	2423 - 2135	Yes
5	2275	2484	2188	2484 - 2188	Yes
6	2136	2296	2052	2296 - 2052	Yes
Toroid	**Bottom View**	**Side-View**			
24 Hours	Diameter (um)	Diameter (Bottom) (um)	Diameter (Top) (um)	Diameter Range (um)	Is Bottom View Within Side View Range?
1	2117	2184	1982	2184 - 1982	Yes
2	2179	2231	1982	2231 - 1982	Yes
3	2105	2118	1982	2118 - 1982	Yes
4	2097	2116	1982	2116 - 1982	Yes
5	2110	2139	1982	2139 - 1982	Yes
6	2120	2112	1982	2112 - 1982	Yes
7	2098	2093	1982	2093 - 1982	No

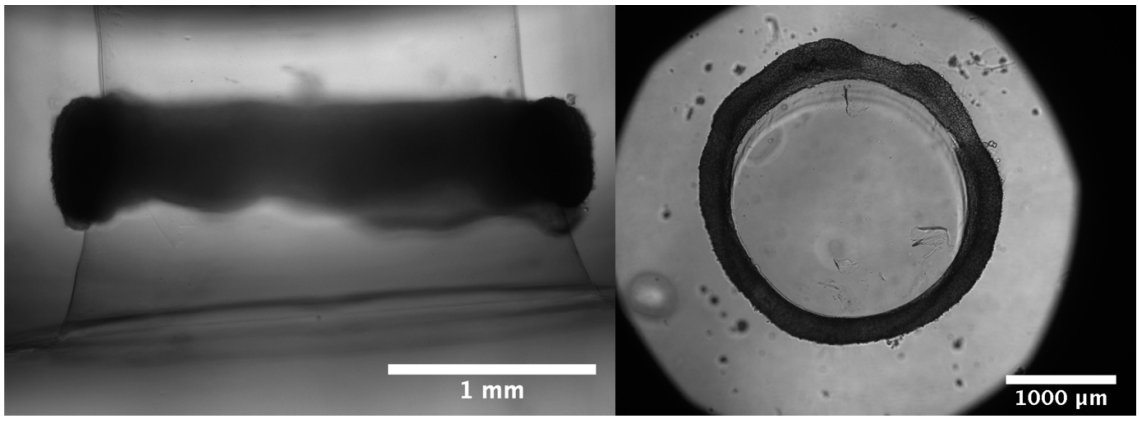

Figure 4.19: Side-view and bottom-view images of same fixed microtissue after 12 hours of contraction within third iteration 75° mold.

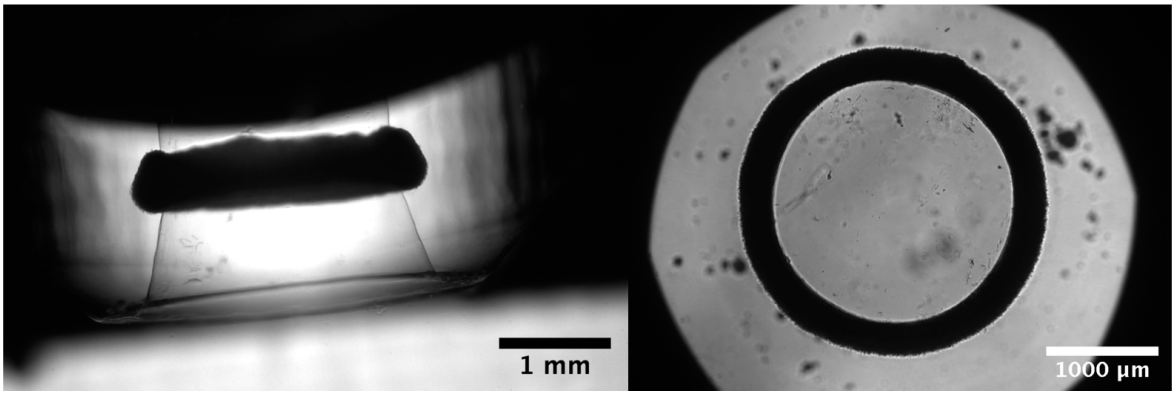

Figure 4.20: Side-view and bottom-view images of same fixed microtissue after 24 hours of contraction within third iteration 75° mold.

4.2 Discussion

4.2.1 Mold Development

The multiple iterations of mold designs represents the evolution and testing of specific design parameters for each mold when self-assembling toroid microtissues. With the first iteration of molds, the purpose of not having a trough was to see its effects on the self-assembly of toroids (Fig. 3.4). In theory, the idea was to remove the amount of space that the toroid microtissues had to self-assemble in order to create a more efficient process. However, during trial runs of the assay, it was observed that cells initially rested at various positions on the ramp, creating random starting positions for toroid contraction. This made comparing toroids within the same trial run a greater challenge. A design parameter that proved successful in the first iteration was the addition of a $90°$ peg at the top of the ramp to prevent the toroid microtissues from falling off the mold. Overall, toroids were able to form and contraction of the microtissues up the ramp was successfully observed.

Having discovered that the toroids started at random points on the $45°$ ramp of the first iteration molds, a $300\,\mu m$ trough was added at the base of the $1\,mm$ ramp (Fig. 3.6). In addition to the trough, the well angle was increased to $45°$ to promote cells settling in the trough when seeding. The trough resolved complications of the first iteration of molds by creating a space where toroids could form off of the ramp and start at similar climbing positions. The second iteration of molds also included $75°$ ramp molds (Fig. 3.5). The purpose was to examine the effects of a 60% increase in ramp steepness would have on the rate of contraction in comparison to the $45°$ ramp molds. It was immediately recognized that after seeding of cells into the $75°$ ramp molds, cells were unable to sit on the ramp during self-assembly of toroids (Fig. 4.7). This was an improvement from the $45°$ ramp molds that still had cells sitting slightly on the ramp during toroid self-assembly (Fig. 4.6). Although more advantageous than the first iteration, it was discovered that the capabilities of the Formlabs 3D printer to print geometries under 500 um was often inaccurate. Certain 3D printed molds had defective trough dimensions, which is unacceptable

for the purposes of the experiment.

Due to the 3D printer being unable to accurately print dimensions under 300um, the trough diameter was increased to 500um. Another reason this was done for the third iteration was to see if toroids would start assembling even further down the ramp or completely in the trough for the $45°$ ramp molds. During the third iteration mold trials it can be seen that toroids started farther down the ramp than the previous two mold iterations for the $45°$ ramp molds (Fig. 4.9). The $500\,\mu m$ trough provided more space for the cells to be seeded into for both the $45°$ and $75°$ molds, creating a reliable starting point off or nearly off of the ramp. The only challenge the user now faces is properly seeding the cells completely around the trough evenly. If not done correctly, more cells will remain on one side causing the toroid to not assemble, instead resulting in one or multiple satellite spheroids. Initial starting position proved to be a vital design element in order to capture the entire window of the toroid self-assembling, becoming stable, and climbing the non-adhesive agarose mold.

An improvement with the third iteration was seeing that when the toroids formed, the different phases of climbing could be seen. After validating the toroid positions, this further proved the non-adhesive mold design validations to be accurate as well with minimal differences in comparison to the original AutoCAD drawings. However, If the molds were to be changed in the future using a more accurate 3D printer, rounded bottom troughs could experimented with instead of flat bottom. With this parameter it could possibly combine design elements of the first iteration and third iteration of molds by promoting self-assembly with greater space off of the angled ramp. The $60°$ ramp mold that was designed could also be introduced as an intermediate ramp height between the $45°$ and $75°$ molds. The essential development of these various molds was to provide an environment that allowed for self-assembly of toroids. All toroids then needed to be able to start at a relatively similar climbing starting point in order to be compared. Microtissues then needed to be able to scale the non-adhesive agarose ramp. Lastly, the toroids needed to remain bound to the peg at the top of the ramp. The third iteration of molds was the most

comprehensive in accomplishing the design parameters set at the beginning of experimentation. Knowing this, the technique of creating these non-adhesive agarose molds is accessible to the average user where they will be able to create accurate molds with ease for their own experiments.

4.2.2 Optimized Toroid Climbing Assay

By verifying that the mold geometries were representative of their original AutoCAD drawings, this allowed for toroid position on the ramp to be reliably recorded. Using bottom-view images, the changing inner lumen area of the toroid microtissues could be tracked for each time-point. These inner lumen areas were then used to calculate the toroid diameter (Equation 4.1) and next the ramp position (Equations 4.2 and 4.2). The position values ($Position_{Ramp}$) could then be graphed over time to follow the microtissue movements up either the $45°$ or $75°$ ramp molds.

The goal of the first iteration trials were to attempt to see if the position of a toroid microtissue using bottom-view could be tracked. Toroids formed on the $45°$ ramp where they rapidly climbed and eventually plateaued near the top (Fig.4.3). By not having to start within a trough or the base of the ramp, toroids had less distance to travel along with not having to contract onto the ramp. This resulted in the shortest total climbing time and a shorter experiment window. By starting on the ramp and having short experiment window, it was believed that certain climbing phenomena may have been missed during first iteration experiments. Overall, the goal of the first iteration was confirmed as toroids did form and could be followed over time.

In conjunction with the first iteration molds being a trial run, creating a working z-depth range that captured the moving microtissue in focus was another important task. As the microtissues climb the ramp, they will inevitably be changing z-heights resulting in the tissue becoming out of focus depending on their position. To counter this, a working range was developed so that for every time point the microtissue would have at least one image that was in focus. This range was generated by examining individual toroids at varying heights and creating a max and min

height (Fig. 4.4). As the toroid changes in and out of focus, another question to answer was how sensitive an accurate z-depth was on calculating area of the lumen. Figure 4.5 showed flexibility of calculating toroid inner lumen area as the toroid changed focus planes. At a single time-point the inner lumen area was measured at the increasing z-heights of 50 um. This exhibited that only when the toroid microtissue was extremely out of focus did the same lumen area seem to change. This was interpreted that the toroid needed to be in focus within reason when measuring and that the z-height was not sensitive enough to have major changes in calculations unless notably out of focus.

The goal of the second iteration molds were to improve upon creating similar initial starting points, test the 75° mold and compare both angled molds climbing positions. Toroids within the 45° molds started at 200 um then slid down the ramp slightly where they recovered and continued to climb over a longer time period than the first iteration 45° molds (Fig. 4.6). Although an improvement on initial starting positions, it would have been more ideal if the starting position was within the trough. 45° molds started on the ramp but the new 75° molds had too steep of a ramp for microtissues to begin on the ramp (Fig. 4.7). 75° Toroids began to self-assemble within the trough before starting to climb the steeper angle. As well as starting in the trough, this was the first time that multiple phases of contraction can be seen using these angled molds. In addition to having multiple phases, the 75° ramp molds had a longer total climbing time than the 45° ramp molds.

During the second iteration, calculating the toroid position was also misunderstood until validation for the third iteration molds. When graphing the toroid positions of mainly the 75° molds, the toroid microtissues were not scaling the full 1000 um ramp (Fig. 4.7). Instead the bases of microtissues appeared to stop at roughly 650 um, leaving an unknown of whether or not the microtissue had completely reached the top. From bottom-view images, it had appeared that the tissues had reached the top, as the tissue looked to be tightly bound to the 90° peg. A realized downside to using bottom-view images is that a user is unable to see the

morphology of the tissue on the ramp other than the changing horizontal thickness. With this gap in understanding, it was hypothesized that the toroids on the 75° molds became more sheath like to scale the higher ramp angle and that upon reaching 650 um, the top of the toroid had reached the 90° peg. With this concept, the toroid was believed to be stuck resting partly on the ramp and on the peg at the same time. After finding that the FormLabs 3D printer was unable to print accurate mold designs below 300 um, microtissue position was not validated and the 300 um mold design was abandoned.

The final third iteration of molds were believed to be the most extensive in applying the previous design parameters. With the extension of the trough to 500 um, the toroid microtissues for the 45° molds started even farther down the ramp with some completely in the trough (Fig. 4.9). The toroids were able to recover and scale the 1000 um ramp. The total climbing time was increased and could be attributed to the lower starting positions on the ramp. The most important observation of the these climbing experiments was the clear distinction of multiple phases of climbing on the 45° molds (Fig. 4.8). This had not previously been seen in past mold iterations and only slightly in the 75° molds before. As the toroid microtissue positions were graphed over time at roughly 3.5 hours toroids appeared to stall on the ramp but not lose position (Fig. 4.9). Microtissues regained momentum after this period and continued to the top of the ramp. As well as with the second iteration 75° molds, the third iteration 75° molds started within the trough (Fig. 4.12). The total climbing time increased to nearly the full 24 hours and an even more significant climbing phase separation was detected.

Much like the second iteration, the third iteration 75° microtissue bases did not reach the top of the ramp (Fig. 4.12). On average they were able to climb to a total of 750 um, similar to the second iteration. The previous hypothesis of why this was happening was that the toroids were becoming sheath like along the steeper ramp angle in order to climb. This hypothesis was based on the comparison of 45° and 75° toroid thicknesses (Fig. 4.10, Fig. 4.13). To further investigate why this was happening, the position validation experiments were conducted (Section 2.6). By

collecting side-view and bottom-view images of the same individual microtissues at 12 and 24 hours, a clear illustration of where the toroids were resting could be created. Here it was found that the diameters calculated from bottom-view did coincide with side-view diameters. Along with both coinciding, it was clear that the 75° toroids had reach the top of the ramp, but were stuck partly on the ramp due to them becoming more sheath like and the 90° peg interfering (Fig. 4.15). This observation also corresponds to the change in thickness calculations, as the 45° microtissues were more thick (Fig. 4.10) when reaching the top of the peg when compared to the 75° microtissues (Fig. 4.13).

After the introduction of the 75° molds it was unclear whether or not the 60% increase in ramp steepness would result in a longer climbing time period in comparison to the 45° molds. It had previously been shown in past literature that even when increasing ramp angles, microtissue cellular forces far outweighed the gravitational forces acting against the toroids climbing (Youssef et al. (2011),Youssef (2012)). These earlier experiments used a minimum ramp height of 55° and a max ramp angle of 85°. When comparing these toroid contractions up the ramps, it resulted in insignificant differences. A key difference from the past experiments with the current climbing assay was the increased size of cells/toroid (25,000 versus 200,000) and a lower ramp angle of 45°. The lower angle and higher seeding density per toroid could have played a role in why significant different total climbing times observed between the 45° and 75° molds.

The most substantial finding of the optimization of the toroid climbing assay was the clear separation of climbing phases for both the 45° and 75° third iteration molds (Fig. 4.9 and Fig. 4.12). A possible theory is that the toroids are able to climb the ramp to the point where they stall using primarily intercellular interactions. An indicator of this was the large decrease in toroid thickness until the point of stalling. After the change in microtissue morphology, the stalling phase could be followed by the fibroblasts remodeling the ECM to further move up the ramp in conjunction with changing morphology. What is actually happening is still unclear during these phases, but possible experiments to solve this include manipulating

individual movement pathways and tracking toroid position over time using the optimized toroid climbing assay.

Chapter 5

Conclusions and Future Directions

The Optimized toroid climbing assay was a proof-of-concept thesis with two fundamental aims: (1) To redesign and validate the non-adhesive agarose climbing molds. (2) To verify that by using a bottom-view imaging process, toroid microtissue contraction can be accurately quantified based on mold geometries. These objectives were established in order to study and improve upon the research of self-assembly and microtissue contraction in a 3D environment.

Chapter 1 consisted of a brief review of the current and past efforts to study toroid microtissue formation. This included explanations on the development of complex microtissues such as toroids and why they are vital parts to developing larger tissue constructs. The cellular forces of these tissues was also discussed and the role of contraction and adhesion in their assembly. Along with developing larger tissues, the importance of the optimized toroid climbing assay for other projects was briefly detailed.

The procedures to accomplishing said objectives for the masters thesis were expressed in chapter 2. Novel molds were designed using AutoCad then 3D printed using a FormLabs Printer. Using the 3D printed plastic molds, the method to cast silicone rubber molds is outlined. From these rubber molds, the creation of non-adhesive agarose molds was characterized. The method to how these molds were then validated is explained. The novel molds were then used to promote and quantify the assembly of toroid microtissues. In order to verify these new molds and tissue formations, a new validation procedure was created and described.

The evolution of different mold iterations were outlined in chapter 3. Here

it explains the goals and purposes of each iteration and how this was accomplished in a step-wise experimental method. The first iteration acted as a trial run, laying out the basics for certain design parameters to be tested and a confirmation that position can be calculated. The next iteration built off of the previous experimental observations where a 75° mold was then introduced. Second iteration molds tested a new 300 um trough and a 60% increase in ramp steepness with the 75° mold. The time and position of the microtissues while climbing were the main focus. The final iteration was the most all-encompassing of iterations. Consisting of both both a 45° and 75° mold with an increased 500 um trough, microtissues started at nearly the same starting point. The total time and behavior of toroid climbing was observed, where different phases were clearly defined.

Chapter 4 described the experimental results and how the qualitative results were used to quantify toroid climbing in combination with each mold iteration. Here it was observed that toroids were able to self-assemble within the novel molds and climb at varying rates dependent on the specific mold geometries. First iteration position calculations revealed that toroids are able to form then rapidly climb a non-adhesive agarose 45° ramp at an exponential rate. Second iteration molds showed that there is a climbing difference between the 45° and 75° toroid microtissues. It was also observed that 75° toroid microtissue bases were unable to reach the top of the ramp. The final iteration built off of the second iteration mold designs with an increase of trough diameter to 500 um. A clear separation of climbing phases was observed for both the 45° and 75° toroids. The third iteration also included a position validation experiment that was necessary to explain the position gap between the top of the ramp and base of the 75° tissues. this position validation experiment also confirmed that bottom-view diameter calculations are in agreement with side-view diameter calculations.

It can be concluded that after the third iteration experiments, the optimization of toroid climbing assay was a successful proof-of-concept. Using bottom-view imaging, inner toroid lumen diameters can be accurately tracked based on defined mold geometries. These important mold geometries were proven to be similar to

the original AutoCAD drawings, creating a reliable source for calculations. From the diameter calculations the position of the bases of the toroids can be followed. By graphing the change in toroid position, one is able to follow the path of the toroids over time as it climbs different angled mold ramps. This process was then verified further by comparing side-view and bottom-view images of the same microtissues and the same time points. From these images both viewpoints gathered similar calculations to one another.

5.1 Future Direction

With the optimized toroid climbing assay showing prosperous results, this creates multiple future projects to improve the assay or other projects. An immediate, necessary future direction is to automate the data collection and analysis. With the current experimental design, microtissues are analyzed manually. For these initial experiments this resulted in a small sample size due to time. It is meticulous and time-consuming, somewhat defeating the purpose of the new assay. A proposed method to do so is create an ImageJ macro capable of running through a stack of bottom-view images and auto-thresholding the images. The most difficult part found in my attempt to create such macro was the thresholding of the different z-positions and how it varied greatly. If solved, a relative center of the mold can be selected and the program could run through a set of images. This would have an output of either the areas or the already calculated diameters and positions. The current 24-well optimized toroid climbing assay could also be considered a proof-of-concept for a 96-well format. Scaling to a 96-well format holds obvious benefits such as more data points, room for experimental procedures at one time, and the possible use of the high-throughput Opera Phoenix microscope. One such limitation as of right now is the lack of automation of analysis that was previously described. With a 24-well format, each trial run generates roughly 300 gigabytes of data. In order to sort through the data generated by the 96-well plate, the procedure must

be automated as well. This entire procedure will also need to be optimized and validated much like the 24-well plate. No biological assays were conducted during the optimization of toroid climbing assay confirmation. This was mainly due to a lack of time to do so, but would be important to further validate the use of the assay. As seen in the third iteration, different phases of climbing were observed but can not be explained by the climbing assay alone. In order to understand what is happening during these different phases, different mediations of contractions could be manipulated, such as Rho kinase (ROCK) contraction. It was hypothesized that the toroids initially climb rapidly due to primarily the cellular interactions of the microtissues forming. They then appeared to stall on the ramp after this rapid thickness decrease, where thickness did not change drastically later in comparison to the earlier phase. With ROCK mediated contraction being important to relaying ECM rigidity, by inhibiting this signal cascade, the last phase of toroid climbing could be explained if the ECM is being remodeled by the toroids in order to further climb up the ramp.

Bibliography

Abbott, Alison (2003). "Biology ' s new dimension". In: *Nature* 424.August, pp. 870–872. URL: http://www.nature.com/nature/journal/v424/n6951/full/424870a.html?foxtrotcallback=true.

Blakely, Andrew M et al. (2015). "Bio-Pick, Place, and Perfuse: A New Instrument for 3D Tissue Engineering." In: *Tissue engineering. Part C, Methods* 21.7, Epub ahead of print. ISSN: 1937-3392 (Electronic). DOI: 10.1089/ten.TEC.2014.0439.

Dean, D.M. et al. (2007). "Rods, tori, and honeycombs: The directed self-assembly of microtissues with prescribed microscale geometries". In: *The FASEB journal : official publication of the Federation of American Societies for Experimental Biology* 21.14, pp. 4005–4012. ISSN: 0892-6638. DOI: 10.1096/fj.07-8710com.

Dean, Dylan M., Adam P. Rago, and Jeffrey R. Morgan (2009). "Fibroblast elongation and dendritic extensions in constrained versus unconstrained microtissues". In: *Cell Motility and the Cytoskeleton* 66.3, pp. 129–141. ISSN: 08861544. DOI: 10.1002/cm.20335.

Elizabeth Leary Sean Curran, Michael Susienka Kali L. Manning Andrew M. Blakely Jeffrey R. Morgan (2017). "Micro-Molded Non-adhesive Hydrogels to Form Multi-cellular Microtissues - The 3D Petri Dish". In: *3D Cell Culture: Technology and Application*, pp. 1–43. ISBN: 6176322472.

Frantz, Christian, Kathleen M Stewart, and Valerie M Weaver (2010). "The extracellular matrix at a glance". In: *Journal of Cell Science* 123.24, 4195 LP –4200. URL: http://jcs.biologists.org/content/123/24/4195.abstract.

Ip, B C et al. (2016). "The bio-gripper: a fluid-driven micro-manipulator of living tissue constructs for additive bio-manufacturing". In: *Biofabrication* 8.2, p. 25015. ISSN: 1758-5090. DOI: 10.1088/1758-5090/8/2/025015. URL: http://dx.doi.org/10.1088/1758-5090/8/2/025015.

Livoti, Christine M and Jeffrey R Morgan (2010). "Minimal Building Units". In: *Tissue Engineering* 16.6, pp. 2051–2061.

Napolitano, Anthony P et al. (2007). "Dynamics of the self-assembly of complex cellular aggregates on micromolded nonadhesive hydrogels." In: *Tissue engineering* 13.8, pp. 2087–2094. ISSN: 1076-3279. DOI: 10.1089/ten.2006.0190.

Rago, Adam P., Dylan M. Dean, and Jeffrey R. Morgan (2009). "Controlling cell position in complex heterotypic 3D microtissues by tissue fusion". In: *Biotechnology and Bioengineering* 102.4, pp. 1231–1241. ISSN: 00063592. DOI: 10.1002/bit.22162.

Tejavibulya, Nalin et al. (2011). "Directed self-assembly of large scaffold-free multicellular honeycomb structures". In: *Biofabrication* 3.3, p. 034110. ISSN: 1758-5082. DOI: 10.1088/1758-5082/3/3/034110. URL: http://iopscience.iop.org/1758-5090/3/3/034110%5Cnhttp://stacks.iop.org/1758-5090/3/i=3/a=034110?key=crossref.0eb23e1261343cc7ae445af97c5

Youssef, Jacquelyn (2012). "Cell Power : Quantifying Cellular Forces in 3D Self-Assembled Microtissues by". PhD thesis. Brown University.

Youssef, Jacquelyn et al. (2011). "Quantification of the forces driving self-assembly of three-dimensional microtissues." In: *Proceedings of the National Academy of Sciences of the United States of America* 108.17, pp. 6993–6998. ISSN: 0027-8424. DOI: 10.1073/pnas.1102559108. URL: http://www.pubmedcentral.nih.gov/articlerender.fcgi?artid=3084067&tool=pmcentrez&rendertype=abstract.

Youssef, Jacquelyn et al. (2012). "Mechanotransduction is enhanced by the synergistic action of heterotypic cell interactions and TGF- 1". In: *The FASEB Journal* 26.6, pp. 2522–2530. ISSN: 0892-6638. DOI: 10.1096/fj.11-199414.

URL: http://www.pubmedcentral.nih.gov/articlerender.fcgi?artid=4052437&tool=pmcentrez&rendertype=abstract%5Cnhttp://www.fasebj.org/cgi/doi/10.1096/fj.11-199414.